Chapter 9

Algorithms for the Euler Equations

9.1 Introduction

The Euler equations describe compressible inviscid flow. Perhaps their most interesting feature is their ability to capture shock waves with the correct entropy increase. At one time there was doubt that numerical solutions of them could accomplish this feat without either viscosity or special shock fitting procedures. Several algorithms for solving the Euler equations are presented herein, some for historical interest and others in general use today. Solutions to a shock tube problem will illustrate their relative merits.

The Euler equations in two dimensions are

$$\frac{\partial U}{\partial t}+\frac{\partial F}{\partial x}+\frac{\partial G}{\partial y}=0$$

where

$$U=\begin{pmatrix}\rho\\ \rho u\\ \rho v\\ e\end{pmatrix},\quad F=\begin{pmatrix}\rho u\\ \rho u^2+p\\ \rho uv\\ (e+p)u\end{pmatrix}\ \text{and}\ G=\begin{pmatrix}\rho v\\ \rho vu\\ \rho v^2+p\\ (e+p)v\end{pmatrix}$$

and $p=p(\rho,\varepsilon)$. For a perfect gas $p=(\gamma-1)\rho\varepsilon$ *with* $\varepsilon=c_vT=\frac{e}{\rho}-\frac{1}{2}(u^2+v^2)$

9.2 The Shock Tube Problem

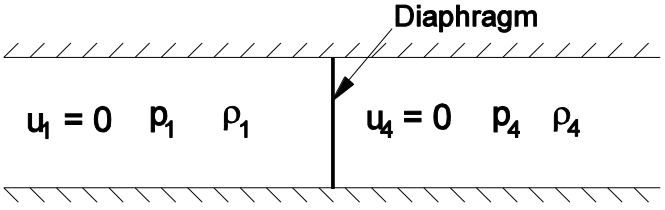

Figure 9.1 Shock tube problem at $t=0$

We will illustrate the numerical algorithms to be presented in this chapter by solving the 1-D Euler equations on the shock tube problem. The unsteady Euler equations in one spatial dimension are

$$\frac{\partial U}{\partial t}+\frac{\partial F}{\partial x}=0,\ \text{where}\ U=\begin{pmatrix}\rho\\ \rho u\\ e\end{pmatrix},\quad F=\begin{pmatrix}\rho u\\ \rho u^2+p\\ (e+p)u\end{pmatrix},\quad \textit{with}\quad \varepsilon=c_vT=\frac{e}{\rho}-\frac{1}{2}u^2$$

The shock tube problem consists initially with the flow at rest and a diaphragm separating two uniform regions at different densities and pressures. The diaphragm is placed at $x=1$ and $\rho=\rho_1$ *and* $p=p_1$ *for* $x<1$ and $\rho=\rho_4$ *and* $p=p_4$ *for* $x\geq 1$. An initial condition is shown in the figure below. At $t=0$ the diaphragm is suddenly broken, sending a shock wave forward and a rarefaction back toward the right boundary. Also, a contact discontinuity, a jump in density, moves slowly forward (toward the left). The exact solution in time is given in Liepmann and Rhosko and in Currie.

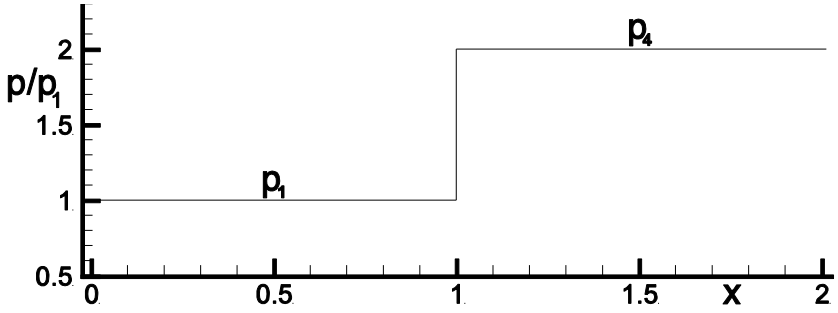

Figure 9.2 Initial condition for pressure

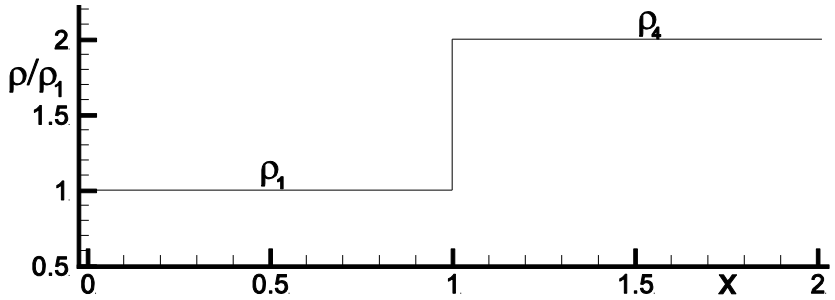

Figure 9.3 Initial condition for density

At t_0 the diaphragm separating the fluid at different pressures and densities disappears. The high pressure side sends a shock wave into the low pressure side leaving a rarefaction in its wake. Between the two sets of waves a contact discontinuity forms as a remnant of the initial density discontinuity. The solutions for pressure density and velocity at a later time are illustrated below.

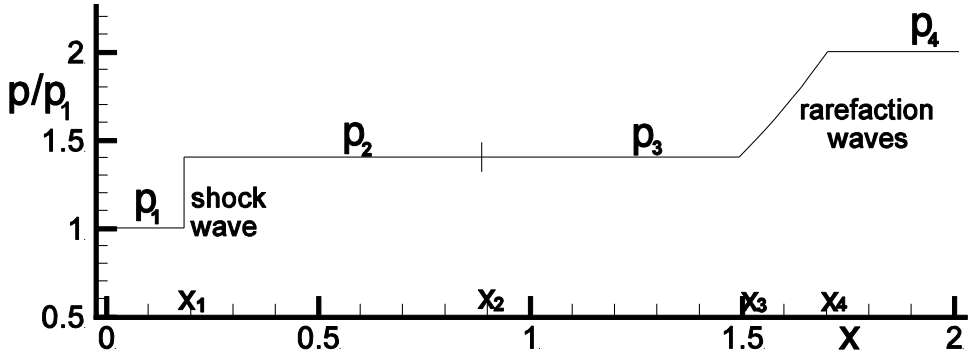

Figure 9.4 Solution for pressure at time $t>t_0$

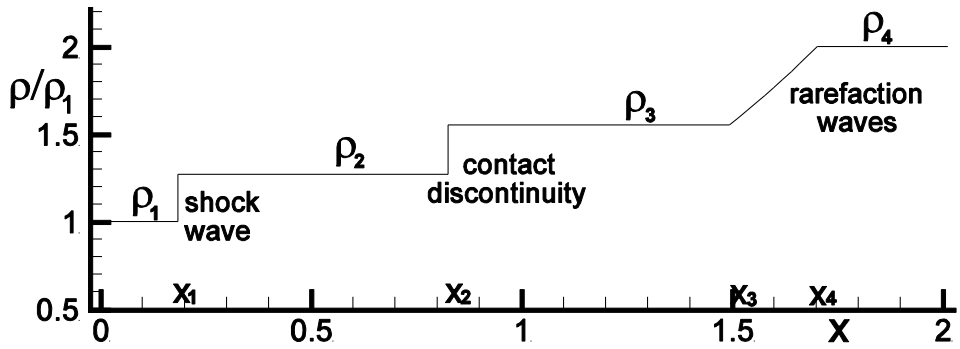

Figure 9.5 Solution for density at time $t > t_0$

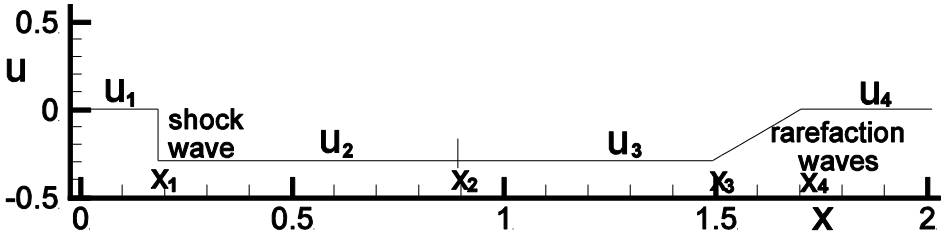

Figure 9.6 Solution for velocity at time $t > t_0$

The above solutions for $p_4 / p_1 = 2$ and $\rho_4 / \rho_1 = 2$ were obtained by first solving the "*shock tube equation"* for the pressure ratio p_2 / p_1 given in Liepmann and Rhosko.

$$\frac{p_4}{p_1} = \frac{p_2}{p_1}\left[1 - \frac{(\gamma-1)(c_1/c_4)(p_2/p_1 - 1)}{\sqrt{2\gamma(2\gamma + (\gamma+1)(p_2/p_1 - 1))}}\right]^{\frac{-2\gamma}{\gamma-1}}$$

Newton's method can be used to solve for the ratio p_2 / p_1 from the known initial conditions, i.e.,. $c_1 = \sqrt{\gamma p_1 / \rho_1}$ and $c_4 = \sqrt{\gamma p_4 / \rho_4}$.

Let $z = p_2 / p_1$ and $f(z) = z\left[1 - \frac{(\gamma-1)(c_1/c_4)(z-1)}{\sqrt{2\gamma(2\gamma + (\gamma+1)(z-1))}}\right]^{\frac{-2\gamma}{\gamma-1}} - \frac{p_4}{p_1}$. Then starting with initial guess $z_1 = \frac{1}{2}\frac{p_4}{p_1}$ iterate $z_{k+1} = z_k - f(z_k)/f'(z_k)$ for $k = 1,...,10$ (see Section 5.3.1 for more on Newton's method). From the converged value for z and the given conditions ahead of the shock wave we can obtain $p_2 = p_3 = zp_1$. From the moving shock relations given in Section 2.4.3.7, we can obtain the following relations for shock wave speed w

$$u_2 = \frac{1}{g}w, \quad \rho_2 = \frac{g}{g-1}\rho_1, \quad w = -\sqrt{\frac{p_2 - p_1}{\rho_1}g}, \quad \text{where} \quad g = \frac{\gamma p_2}{p_2 - p_1} - \frac{\gamma - 1}{2}$$

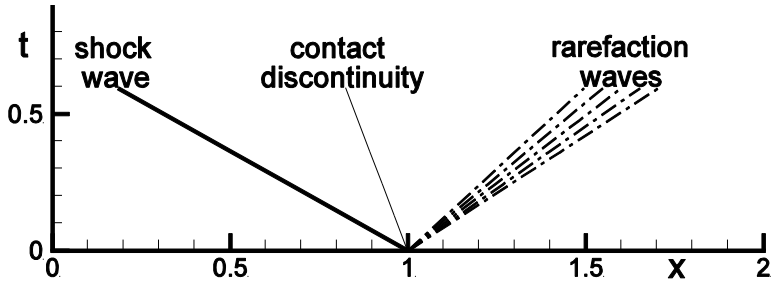

Figure 9.7 Wave progression in time

The shock wave position is given by $x_1 = 1 + w(t - t_0)$ and that for the contact discontinuity by $x_2 = 1 + u_2(t - t_0)$. The flow through the set of rarefaction waves is isentropic and ρ_3, the density to the left of the rarefaction, is given by $\rho_3 = \rho_4 (p_3 / p_4)^{1/\gamma}$. The set of rarefaction waves are bounded by $x_3 = 1 + (u_3 + c_3)(t - t_0)$, with $c_3 = \sqrt{\gamma p_3 / \rho_3}$, and $x_4 = 1 + c_4(t - t_0)$. The velocity u increases linearly between x_3 and x_4. The pressures and densities can be found in this region by the relations (see also Currie or Liepmann and Rhosko)

$$\rho = \rho_4 \left[1 - \frac{\gamma - 1}{2} \frac{|u|}{c_4} \right]^{\frac{2}{\gamma - 1}} \text{ and } p = p_4 \left[1 - \frac{\gamma - 1}{2} \frac{|u|}{c_4} \right]^{\frac{2\gamma}{\gamma - 1}}$$

For the algorithm applications to follow, if the pressure and density p_1 and ρ_1 are at atmospheric conditions, $p_1 = 1.01325 x 10^5 N/m^2$ and $\rho_1 = 1.225 kg/m^3$, the ratios p_4 / p_1 and ρ_4 / ρ_1 equal 2 and the speeds $u_1 = u_4 = 0$, then $\rho_2 = 1.568 kg/m^3$, $p_2 = 1.420 \times 10^5 N/m^2$, $\rho_3 = 1.914 kg/m^3$, $p_3 = 1.420 \times 10^5 N/m^2$, $u_3 = -83.94 m/s$ and $w = -393.2 m/s$.

9.3 The MacCormack Method (1969)

An explicit two step, predictor-corrector, method for solving the above equation is

$$p: \quad \overline{U_{i,j}^{n+1}} = U_{i,j}^n - \Delta t \left(\frac{D_+ \cdot}{\Delta x} F_{i,j}^n + \frac{D_+ \cdot}{\Delta y} G_{i,j}^n \right)$$

$$c: \quad U_{i,j}^{n+1} = \frac{1}{2} \left\{ U_{i,j}^n + \overline{U_{i,j}^{n+1}} - \Delta t \left(\frac{D_- \cdot}{\Delta x} \overline{F_{i,j}^{n+1}} + \frac{D_- \cdot}{\Delta y} \overline{G_{i,j}^{n+1}} \right) \right\}$$

In the above equations, forward difference approximations are used for spatial derivatives in the predictor step and are followed by backward difference approximations in the corrector step. The net result is equivalent to a second order accurate central difference approximation. Backward difference approximations or a mixed combination could also have been used in the predictor step followed by correspondingly opposite one sided difference approximations in the corrector step. The averaging of the spatial difference approximations at times $n\Delta t$ and $(n+1)\Delta t$ in the

second step effectively centers the method in time as well as in space. The method is second order accurate.

In one spatial dimension, for example the x direction, it is not too difficult to show that the above numerical method is stable if the time step satisfies the following CFL condition.

$$\Delta t \le \frac{\Delta x}{|u|+c}, \quad with \quad |u|+c = \|A\| \quad and \quad A = \frac{\partial F}{\partial U}$$

No proof of stability exists in two or three dimensions for the above method. However, the following CFL condition based on the geometrical constraint of enclosing the physical domain of dependence within the numerical domain defined by the mesh points $(i+1, j)$, $(i-1, j)$, $(i, j+1)$ and $(i, j-1)$ is often used.

$$\Delta t \le \frac{1}{\frac{|u|}{\Delta x} + \frac{|v|}{\Delta y} + c\sqrt{\frac{1}{\Delta x^2} + \frac{1}{\Delta y^2}}}$$

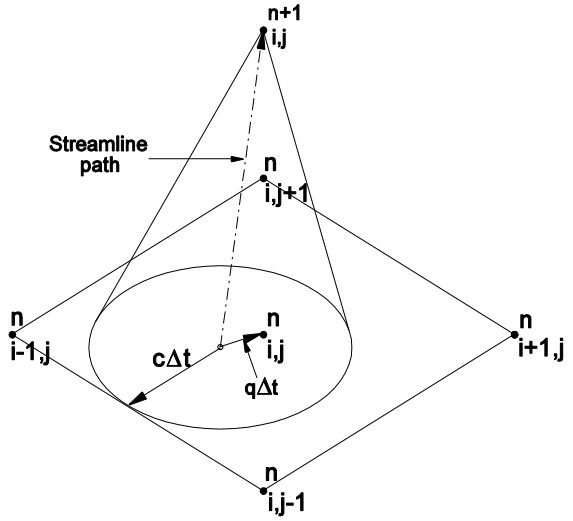

Figure 9.8 Geometric cone of dependence constraint for numerical stability.

The extension to three dimensions is straight forward. Because of the choice of forward or backward difference approximations in each of the two steps, there are 2^d different choices for the method in a space of dimension d. To avoid a preferred spatial direction, and perhaps to enhance numerical stability, it is recommended that each variation be cycled through during the course of a long calculation.

This two step procedure, with each step different, produces a pseudo-unsteadiness preventing the method from converging below the truncation error of the algorithm to machine zero. Machine zero is of the order of the noise, or the randomness of the last bit of a machine word in the mathematics of the finite word size numbers used within digital computers. Single step algorithms on the other hand, and also some multi step algorithms that use the same type of difference approximation for each step, can converge well below their truncation error to machine zero.

9.3.1 Exercise: Calculate the flow within a shock tube Solve the 1-D Euler equations with the MacCormack method. The shock tube problem consists initially with the flow at rest with a diaphragm separating two uniform regions at different densities and pressures. Place the

diaphragm at $x=1$ and let $\rho=\rho_0$ and $p=p_0$ for $x<1$ and $\rho=2\rho_0$ *and* $p=2p_0$ *for* $x\geq 1$, where $\rho_0=1kg/m^3$ and $p_0=1\times10^5 N/m^2$. Use 81 mesh points to span the region $0\leq x\leq 2$ and $\Delta t=0.9\left.\dfrac{\Delta x}{|u|+c}\right|_{\min}$. The chosen CFL number of 0.9 represents a small safety factor below unity. The initial condition is shown in the figure below. At $t=0$ the diaphragm is suddenly broken sending a shock wave forward and a rarefaction back toward the exit. Also, a contact discontinuity, a jump in density, moves slowly forward. The calculation is to be stopped before either wave reaches a boundary, thereby fixing the boundary values to their initial values.

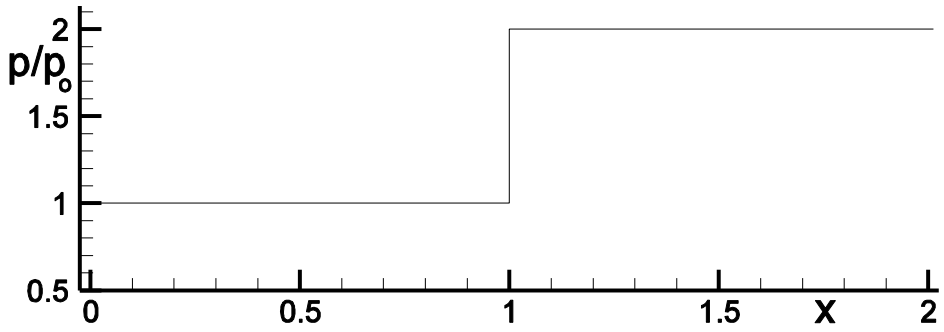

Figure 9.9 Initial condition for pressure

The numerical solution (solid symbols) is compared with the exact solution (see, for example, Liepmann and Roshko) for pressure and density below after 40 time steps.

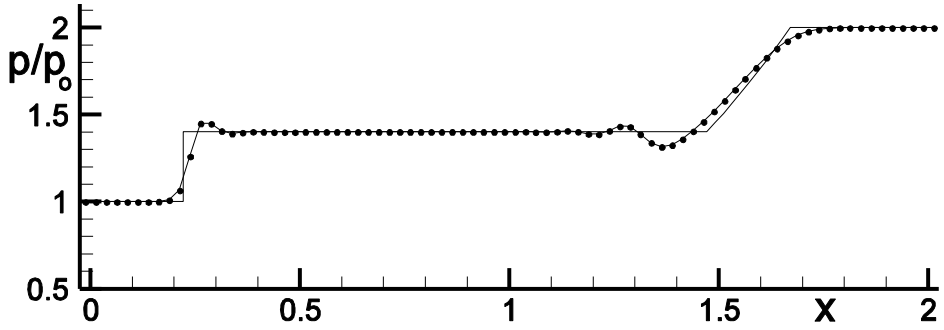

Figure 9.10 Pressure comparison

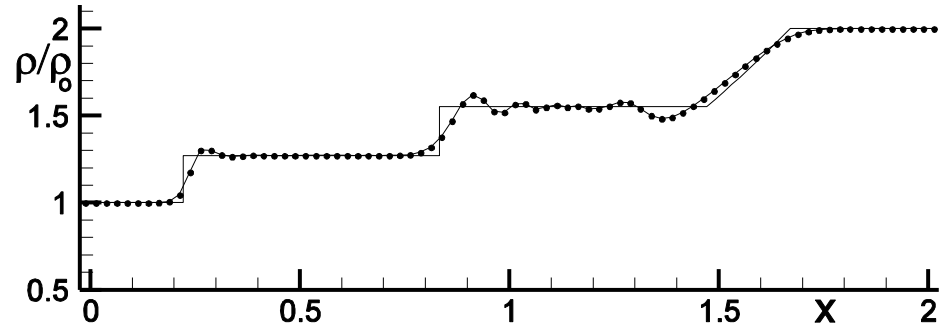

Figure 9.11 Density comparison

Note that there is oscillation in the solution at the discontinuities. This is unavoidable for second order or higher accuracy algorithm without a flux limiter. This is the Gibbs phenomena seen when approximating a step discontinuity with a finite Fourier series. Note also that the shock wave is steeper than the contact discontinuity. The shock wave is a nonlinear discontinuity with the self steepening mechanism described in Section 5.2.3 and the contact discontinuity acts more like a linear discontinuity. The figure below shows the characteristic paths for the characteristic speed $u+c$. Note the converging paths at the shock near $x=0.2$ and the diverging paths in the rarefaction region, at about $x=1.5$. Note also the weaker convergence in the vicinity of the contact discontinuity near $x=0.8$.

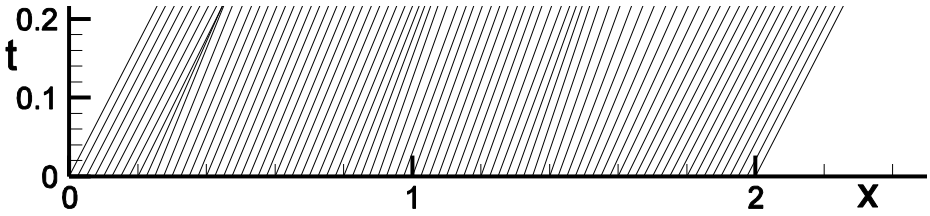

Figure 9.12 The $u+c$ characteristic paths

9.4 The Beam and Warming Method (1975--76)

A Crank-Nicolson like implicit approximation to the Euler equations is given below

$$U_{i,j}^{n+1} = U_{i,j}^{n} - \frac{\Delta t}{2}\left\{\left(\frac{D_0\cdot}{\Delta x}F_{i,j}^{n} + \frac{D_0\cdot}{\Delta y}G_{i,j}^{n}\right) + \left(\frac{D_0\cdot}{\Delta x}F_{i,j}^{n+1} + \frac{D_0\cdot}{\Delta y}G_{i,j}^{n+1}\right)\right\}$$

The above numerical approximation is centered in both space and time and is second order accurate. The fundamental difficulty in directly implementing the above algorithm is in determining the functions $F(U)$ and $G(U)$ at time $(n+1)\Delta t$. If these functions were linear, we could express them as $F=AU$ and $G=BU$, where A and B are matrices independent of U, and then solve a block matrix equation for the unknown solution U at time $(n+1)\Delta t$. In general, the functions F and G are nonlinear functions of the elements of U and therefore must first be linearized.

By Taylor series expansion

$$F_{i,j}^{n+1} = F_{i,j}^{n} + \left.\frac{\partial F}{\partial U}\right|_{i,j}^{n} \underbrace{\left(U_{i,j}^{n+1} - U_{i,j}^{n}\right)}_{\approx \Delta t\frac{\partial U}{\partial t}} + \textit{higher order terms}$$

where $\left.\dfrac{\partial F}{\partial U}\right|_{i,j}^{n} = A_{i,j}^{n}$, the Jacobian of F with respect to U.

Note that the second term on the right is of first order in Δt. The higher order terms that are to be neglected are of second and higher orders.

Similarly,

$$G_{i,j}^{n+1} = G_{i,j}^{n} + \left.\frac{\partial G}{\partial U}\right|_{i,j}^{n} \left(U_{i,j}^{n+1} - U_{i,j}^{n}\right) + \textit{higher order terms}$$

$$B_{i,j}^{n}$$

We define $\delta U_{i,j}^{n+1} = U_{i,j}^{n+1} - U_{i,j}^{n}$

Note: We will use the "lower case" delta to denote the change in the solution computed implicitly, and the "triangle" Delta to denote the solution change computed explicitly.

Using only the first two terms of the above expansions for F and G

$$\frac{D_0 \cdot}{\Delta x} F_{i,j}^{n+1} + \frac{D_0 \cdot}{\Delta y} G_{i,j}^{n+1} = \frac{D_0 \cdot}{\Delta x} F_{i,j}^{n} + \frac{D_0 \cdot}{\Delta y} G_{i,j}^{n} + \frac{D_0 \cdot}{\Delta x} A_{i,j}^{n} \delta U_{i,j}^{n+1} + \frac{D_0 \cdot}{\Delta y} B_{i,j}^{n} \delta U_{i,j}^{n+1}$$

By substitution the difference equation becomes

$$U_{i,j}^{n+1} = U_{i,j}^{n} - \underbrace{\Delta t \left(\frac{D_0 \cdot}{\Delta x} F_{i,j}^{n} + \frac{D_0 \cdot}{\Delta y} G_{i,j}^{n} \right)}_{\Delta U_{i,j}^{n}} - \frac{\Delta t}{2} \left(\frac{D_0 \cdot}{\Delta x} A_{i,j}^{n} + \frac{D_0 \cdot}{\Delta y} B_{i,j}^{n} \right) \delta U_{i,j}^{n+1}$$

where the dots appearing in the difference operators imply that the operators operates on all factors to the right, including the factor $\delta U_{i,j}^{n+1}$. This equation can be rewritten in "delta" law form as

$$\left\{ I + \frac{\Delta t}{2} \left(\frac{D_0 \cdot}{\Delta x} A_{i,j}^{n} + \frac{D_0 \cdot}{\Delta y} B_{i,j}^{n} \right) \right\} \delta U_{i,j}^{n+1} = \Delta U_{i,j}^{n}$$

Note that the neglected terms in the expansions of F and G would have only contributed to terms of third order. Therefore the above approximation retains the second order accuracy of the original implicit difference equation.

The solution of the above implicit equation requires the inversion of the bracketed factor on the left hand side. This factor represents a block pentadiagonal matrix whose diagonals are not all adjacent. There is no efficient procedure available to invert this type of matrix. Instead, it is approximately factored into two simpler block tridiagonal matrix factors, each of which has an efficient inverse procedure as follows.

$$\left\{ I + \frac{\Delta t}{2} \frac{D_0 \cdot}{\Delta x} A_{i,j}^{n} \right\} \left\{ I + \frac{\Delta t}{2} \frac{D_0 \cdot}{\Delta y} B_{i,j}^{n} \right\} \delta U_{i,j}^{n+1} = \Delta U_{i,j}^{n}$$

If we multiply the two factors together we obtain, in addition to what we started with, the following error term introduced by approximate factorization

$$\frac{\Delta t^2}{4}\frac{D_0\cdot}{\Delta x}A^n_{i,j}\frac{D_0\cdot}{\Delta y}B^n_{i,j}\,\delta U^{n+1}_{i,j}$$

Again, because $\delta U^{n+1}_{i,j} \approx \Delta t \left.\frac{\partial U}{\partial t}\right|^n_{i,j}$ this term is also of third order, and therefore the above factored difference equation is still of second order accuracy. The norm of the introduced error term is approximately equal to the product of two one-dimensional CFL numbers times a second difference of the solution change as shown below

$$\frac{\Delta t\|A\|}{\Delta x}\frac{\Delta t\|B\|}{\Delta y}\frac{1}{4}D_0^2\cdot\delta U^n_{i,j}$$

The reason for using an implicit method is to be able to take large time steps not subject to the CFL stability conditions of explicit methods. However, as can be seen above, the time step can be limited by accuracy conditions. This limitation can be severe during the initial transient part of the calculation.

The solution of the approximately factored difference equation is similar to that presented in Section 5.2.2, except 5x5 block element matrices replace the former scalar elements of the tridiagonal matrix. Chapter 11 will present the details of the matrix inversion procedure sketched below.

(1) Let $\delta U^*_{i,j} = \left\{I + \frac{\Delta t}{2}\frac{D_0\cdot}{\Delta y}B^n_{i,j}\right\}\delta U^{n+1}_{i,j}$ and then the following block tridiagonal matrix equation is solved for $\delta U^*_{i,j}$.

$$\left\{I + \frac{\Delta t}{2}\frac{D_0\cdot}{\Delta x}A^n_{i,j}\right\}\delta U^*_{i,j} = \Delta U^n_{i,j}$$

(2) Now that $\delta U^*_{i,j}$ is known, the following block tridiagonal equation for is solved for $\delta U^{n+1}_{i,j}$.

$$\left\{I + \frac{\Delta t}{2}\frac{D_0\cdot}{\Delta y}B^n_{i,j}\right\}\delta U^{n+1}_{i,j} = \delta U^*_{i,j}$$

(3) Knowing $\delta U^{n+1}_{i,j}$, the solution can be updated and the calculation continued for another time step.

$$U^{n+1}_{i,j} = U^n_{i,j} + \delta U^{n+1}_{i,j}$$

A generalized form for the Beam and Warming method (1978) is given below

$$\delta U_{i,j}^{n+1} = \frac{-\theta_1}{1+\theta_2}\Delta t\left(\frac{D_0\cdot}{\Delta x}A_{i,j}^n + \frac{D_0\cdot}{\Delta y}B_{i,j}^n\right)\delta U_{i,j}^{n+1} - \frac{\Delta t}{1+\theta_2}\left(\frac{D_0\cdot}{\Delta x}F_{i,j}^n + \frac{D_0\cdot}{\Delta y}G_{i,j}^n\right) + \frac{\theta_2}{1+\theta_2}\delta U_{i,j}^n$$

Case 1. $\theta_1 = 1/2$ *and* $\theta_2 = 0$ - This special form given earlier is second order accurate and neutrally stable.

Case 2. $\theta_1 = 1$ *and* $\theta_2 = 0$ - This algorithm is fully implicit, first order accurate, and unconditionally stable.

Case 3. $\theta_1 = 1$ *and* $\theta_2 = 1/2$ - This three point backward implicit algorithm is second order accurate and unconditionally stable.

The extension of the Beam and Warming method to three-dimensional flows has been theoretically shown to be unstable, although not observed in use, because the method is usually used together with numerical dissipation terms to control instabilities, even in one- or two-dimensional applications. The method has been very popular since its introduction and has been used successfully to solve a wide range of problems in fluid dynamics in one, two, and three dimensions.

9.4.1 Exercise: Calculate the flow within the shock tube problem given in Section 9.2 using the Beam and Warming method. The results for a CFL number of 0.9, after 40 time steps, using the Case 1 form of the algorithm are shown below.

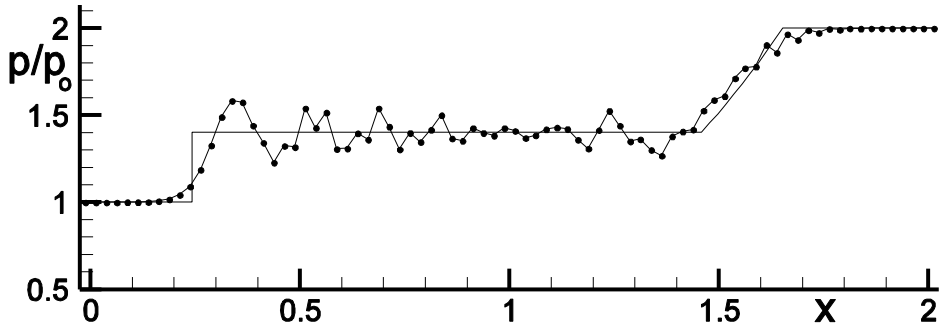

Figure 9.13 Pressure comparison, Case1 form

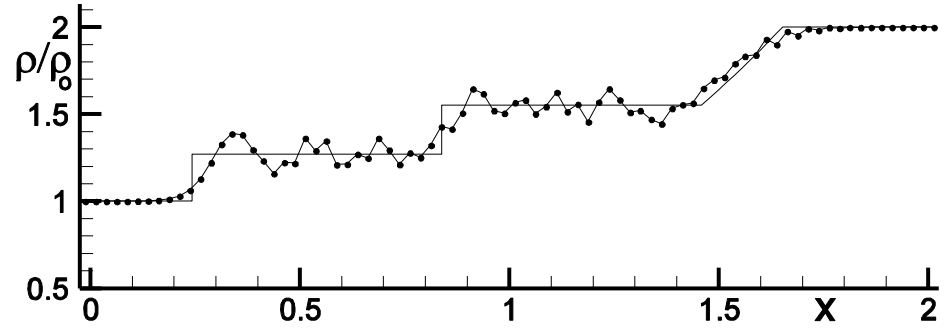

Figure 9.14 Density comparison, Case1 form

9.4.2 Artificial Dissipation

Note the "saw tooth" error appearing in the solution. Central difference schemes are blind to "saw tooth" disturbances because the solution at odd indices of "i" depend only upon even indices of "i" and vice versa. They can be controlled by adding artificial viscosity to the fluxes, as shown below. First, the explicit term can be expressed as

$$\left(\frac{D_0\cdot}{\Delta x}F^n_{i,j}+\frac{D_0\cdot}{\Delta y}G^n_{i,j}\right)=\left(\frac{F^n_{i+1/2,j}-F^n_{i-1/2,j}}{\Delta x}+\frac{G^n_{i,j+1/2}-G^n_{i,j-1/2}}{\Delta x}\right)$$

$$\text{with } F^n_{i+1/2,j}=\frac{1}{2}(F^n_{i,j}+F^n_{i+1,j}) \text{ and } G^n_{i,j+1/2}=\frac{1}{2}(G^n_{i,j}+G^n_{i,j+1}) \text{ etc.}$$

Then the fluxes are modified to include viscous terms as follows

$$F^n_{i+1/2,j}\leftarrow\frac{1}{2}(F^n_{i,j}+F^n_{i+1,j})-\varepsilon(|u_{i+1/2,j}|+c_{i+1/2,j})\left(U^n_{i+1,j}-U^n_{i,j}\right)$$

$$G^n_{i,j+1/2}\leftarrow\frac{1}{2}(G^n_{i,j}+G^n_{i,j+1})-\varepsilon(|v_{i,j+1/2}|+c_{i,j+1/2})\left(U^n_{i,j+1}-U^n_{i,j}\right)$$

where ε, usually a small positive number in the range $0\le\varepsilon\le1$, is chosen sufficiently large to remove the unwanted numerical error. The velocity factors above are introduced to keep the fluxes dimensionally correct and to give the artificial viscous term weight proportional to the Euler terms. Similarly, the corresponding implicit terms need modification, as follows.

$$\left(\frac{D_0\cdot}{\Delta x}A^n_{i,j}+\frac{D_0\cdot}{\Delta y}B^n_{i,j}\right)\leftarrow$$

$$\left(\frac{D_0\cdot}{\Delta x}A^n_{i,j}+\frac{D_0\cdot}{\Delta y}B^n_{i,j}-\varepsilon\Delta x\frac{D_+\cdot}{\Delta x}\frac{D_-\cdot}{\Delta x}(|u_{i,j}|+c_{i,j})-\varepsilon\Delta y\frac{D_+\cdot}{\Delta y}\frac{D_-\cdot}{\Delta y}(|v_{i,j}|+c_{i,j})\right)$$

This modification adds artificial viscosity terms

$$\Delta t\frac{\partial\nu_x\dfrac{\partial U}{\partial x}}{\partial x}+\Delta t\frac{\partial\nu_y\dfrac{\partial U}{\partial y}}{\partial y}\text{, with } \nu_x=\varepsilon\Delta x(|u|+c) \text{ and } \nu_y=\varepsilon\Delta y(|v|+c),$$

to the difference equation. These terms are of order $O(\varepsilon\Delta t\Delta x,\varepsilon\Delta t\Delta y)$, perhaps compromising second order accuracy. Third order dissipation terms could and perhaps should be added instead, but the examples to follow use the approach given above.

An alternative procedure to increasing the order of the artificial viscosity terms and target them to regions of solution oscillation is to make ε depend upon the strength of the oscillation itself. For example, we first write the artificial viscous term in the x-direction, in conservation form, as

$$\varepsilon\Delta x\frac{D_+}{\Delta x}\cdot\frac{D_-}{\Delta x}(|u_{i,j}|+c_{i,j})U_{i,j}=\frac{D_+\cdot\nu_{i+1/2,j}\dfrac{D_-\cdot U_{i,j}}{\Delta x}}{\Delta x}=\frac{\nu_{i+1/2,j}(U_{i+1,j}-U_{i,j})-\nu_{i-1/2,j}(U_{i,j}-U_{i-1,j})}{\Delta x^2}$$

$$\text{and define}\quad \nu_{i+1/2,j}=\underbrace{\varepsilon\frac{|p_{i+1}-2p_i+p_{i-1}|}{p_{i+1}+2p_i+p_{i-1}}}_{new\ \varepsilon}\Delta x\frac{1}{2}(|u_i|+c_i+|u_{i+1}|+c_{i+1})$$

The "new ε" now depends upon an approximation to the second derivative of pressure and is proportional to $\varepsilon\Delta x^2\dfrac{1}{4p}\dfrac{\partial^2 p}{\partial x^2}$. Note also that the pressure quotient term multiplying ε can never be greater than one, as long as pressure stays positive.. The y-direction artificial viscous term can be similarly treated.

The above calculation was repeated with $\varepsilon=1/8$, but with no pressure quotient factor. The results are shown below. The results appear much better now. Note the "hump" at the shock, which is characteristic of second order methods.

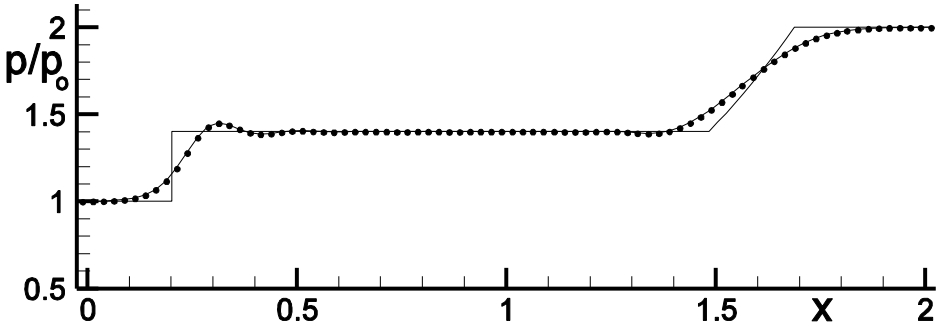

Figure 9.15 Pressure comparison, Case 1 form with $\varepsilon=1/8$

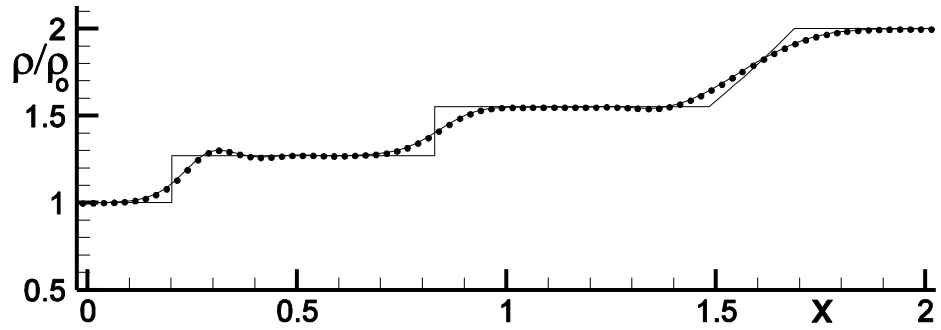

Figure 9.16 Density comparison, Case1 form with $\varepsilon=1/8$

Density results for the Case 2 form of the Beam and Warming algorithm, also with $\varepsilon=1/8$ are shown below.

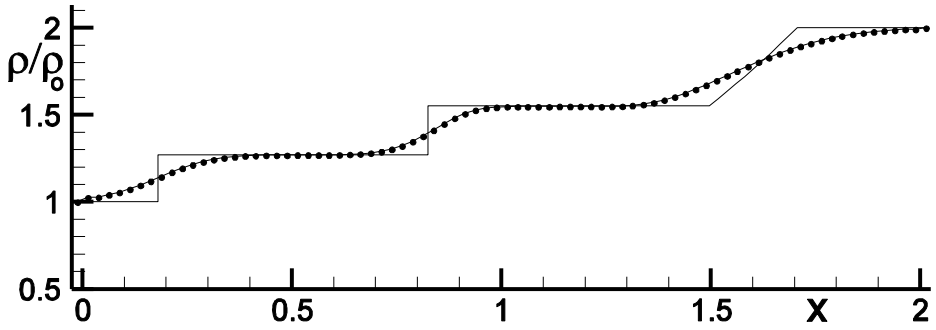

Figure 9.17 Density comparison, Case 2 form with $\varepsilon = 1/8$

Note the monotonic results above for the Case 2 form of the fully implicit first order accurate algorithm. The density results for the three point backward in time, second order accurate, algorithm are shown below.

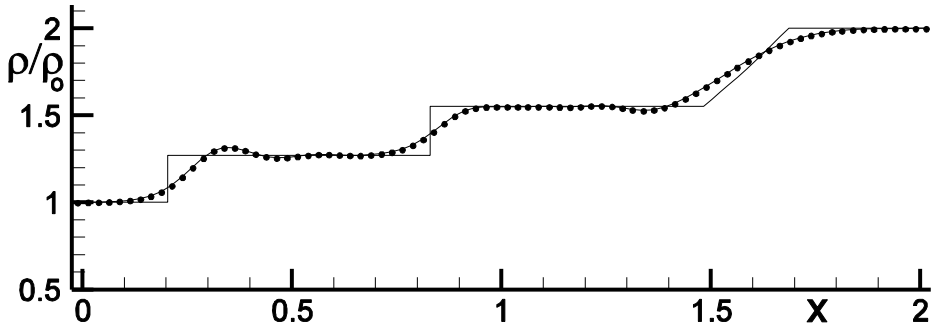

Figure 9.18 Density comparison, Case 3 form with $\varepsilon = 1/8$

The above results for the Beam and Warming algorithm have all been for a CFL number of 0.9. But, this implicit method is not bounded by CFL numbers less than one. The results for CFL numbers of 1.8 for 20 time steps and 3.6 for 10 time steps are shown below.

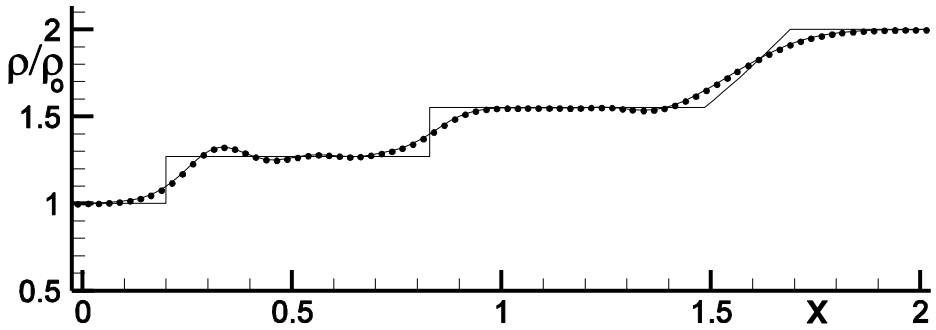

Figure 9.19 Density comparison, Case 1 form with $\varepsilon = 1/8$, CFL=1.8, 20 time steps

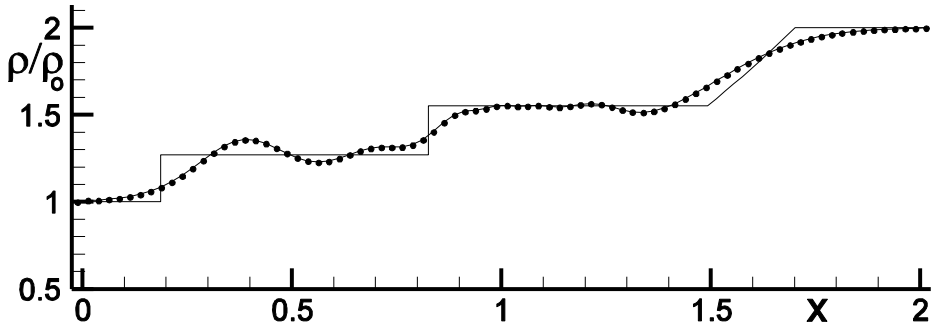

Figure 9.20 Density comparison, Case 1 form with $\varepsilon = 1/8$, CFL=3.6, 10 time steps

The solutions are seen to deteriorate with increased CFL numbers. However, there are optimal choices, depending upon the particular flow problem. This problem contains a moving shock wave, which will limit the CFL to a lower value than for a flow converging to a steady state.

9.4.2.1 Artificial or Genuine Dissipation

A further distinction can be made on numerical dissipation. If a term, conjured up to promote enhanced numerical dissipation, is added to the difference equations, then it should be called artificial. On the other hand, if terms of the original set of differential equations are approximated by for example by upwind differencing, which also enhances dissipation, it is less artificial and perhaps should be called genuine. All approximated derivative terms can be viewed as central differencing plus a dissipation term. For example, consider a backward difference approximation to

$$-c\frac{\partial u}{\partial x} \approx -c\frac{u_i - u_{i-1}}{\Delta x} = -c\frac{u_{i+1} - u_{i-1}}{2\Delta x} + c\frac{u_{i+1} - 2u_i + u_{i-1}}{2\Delta x}$$

9.5 The Jameson Runge-Kutta Method

Jameson presented the following Runge-Kutta-like scheme for solving the Euler equations

$$U_{i,j}^{(0)} = U_{i,j}^{n}$$

$$U_{i,j}^{(k)} = U_{i,j}^{n} - \alpha_k \Delta t\left(\frac{D_0 \cdot}{\Delta x}F_{i,j}^{(k-1)} + \frac{D_0 \cdot}{\Delta y}G_{i,j}^{(k-1)}\right) \quad with \quad \alpha_k = \frac{1}{5-k}, \quad for \quad k = 1,2,3,4$$

$$U_{i,j}^{n+1} = U_{i,j}^{(4)}$$

Like the Beam-Warming method, it uses central difference approximations for all spatial derivatives, but it is explicit with the following less restrictive CFL condition.

$$\Delta t \le \frac{2\sqrt{2}}{\frac{|u|}{\Delta x} + \frac{|v|}{\Delta y} + c\sqrt{\frac{1}{\Delta x^2} + \frac{1}{\Delta y^2}}}$$

The method is fourth order accurate in time and second order accurate in space. Again, because central difference schemes are blind to "saw tooth" disturbances, dissipative terms need to be

added to control the growth of numerical error. The fluxes are modified to include artificial viscous terms, as before for the Beam and Warming method of the last section. These terms, which are illustrated below, also use an ε, but should be bounded by $0 \le \varepsilon \le 1/4$ for stability.

$$\left(\frac{D_0 \cdot}{\Delta x} F_{i,j}^{(k)} + \frac{D_0 \cdot}{\Delta y} G_{i,j}^{(k)} \right) = \left(\frac{F_{i+1/2,j}^{(k)} - F_{i-1/2,j}^{(k)}}{\Delta x} + \frac{G_{i,j+1/2}^{(k)} - G_{i,j-1/2}^{(k)}}{\Delta x} \right)$$

$$F_{i+1/2,j}^{(k)} \leftarrow \frac{1}{2}(F_{i,j}^{(k)} + F_{i+1,j}^{(k)}) - \varepsilon\left(\left|u_{i+1/2,j}^{(k)}\right| + c_{i+1/2,j}^{(k)}\right)\left(U_{i+1,j}^{(k)} - U_{i,j}^{(k)}\right)$$

$$G_{i,j+1/2}^{(k)} \leftarrow \frac{1}{2}(G_{i,j}^{(k)} + G_{i,j+1}^{(k)}) - \varepsilon\left(\left|v_{i,j+1/2}^{(k)}\right| + c_{i,j+1/2}^{(k)}\right)\left(U_{i,j+1}^{(k)} - U_{i,j}^{(k)}\right)$$

9.5.1 Exercise: Calculate the flow within the shock tube problem given in Section 9.2 using the Jameson Runge-Kutta three step method. The density results, after 40 time steps, with $\varepsilon = 1/8$, are shown in Figure 9.21 for a CFL number of 0.9 and in Figure 9.22 for a CFL number of 1.8, after 20 time steps, with $\varepsilon = 1/4$.

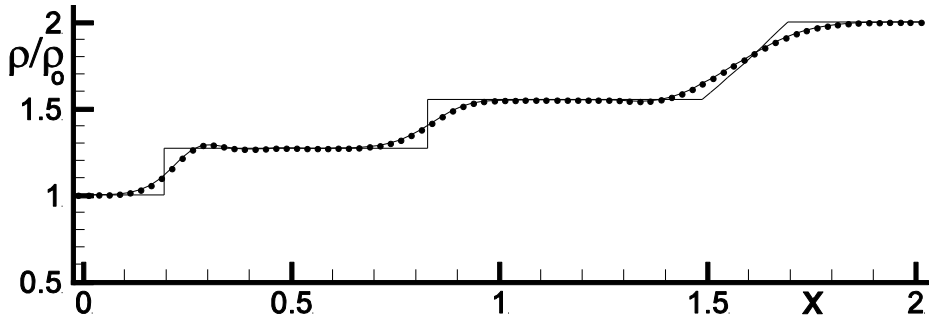

Figure 9.21 Density comparison, JRK four step method with CFL=0.9 and $\varepsilon = 1/8$

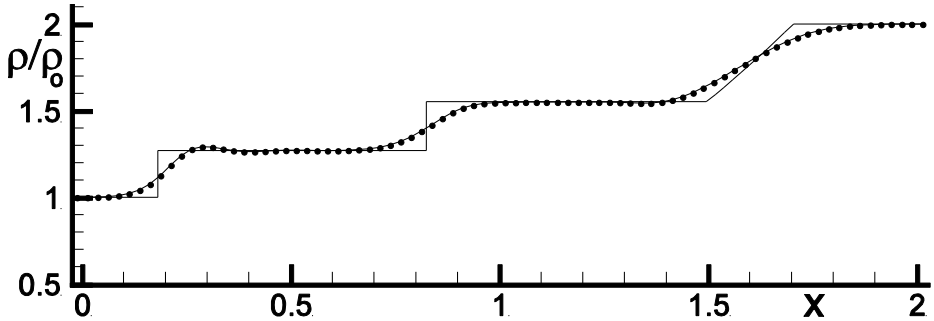

Figure 9.22 Density comparison, JRK four step method with CFL=1.8 and $\varepsilon = 1/8$

Jameson also advises "residual averaging" when applying the above algorithm. This means that the solution changes $\Delta U_{i,j}^n = U_{i,j}^{n+1} - U_{i,j}^n$ are averaged locally as follows

$$\Delta U_{i,j}^n \leftarrow \left\{ I + \varepsilon \left(\Delta x^2 \frac{D_+ \cdot}{\Delta x} \frac{D_- \cdot}{\Delta x} + \Delta y^2 \frac{D_+ \cdot}{\Delta y} \frac{D_- \cdot}{\Delta y} \right) \right\} \Delta U_{i,j}^n, \quad \varepsilon \approx 1/8$$

By averaging the residuals instead implicitly, the Jameson method becomes a very stable and numerically efficient method as follows.

$$\left\{ I + \varepsilon \left(\Delta x^2 \frac{D_+ \cdot}{\Delta x} \frac{D_- \cdot}{\Delta x} + \Delta y^2 \frac{D_+ \cdot}{\Delta y} \frac{D_- \cdot}{\Delta y} \right) \right\} \delta U_{i,j}^{n+1} = \Delta U_{i,j}^{n}, \quad \varepsilon > 0$$

For solutions converging to a steady state, Jameson suggests using, instead of the same value for the time step everywhere, time step sizes that are determined locally. That is, each mesh point has a different time step size determined from the local CFL condition. This idea was originally introduced by C. P. Li ("Numerical Solution of Viscous Reacting Blunt Flows of a Multi-Component Mixture", AIAA Paper No.73-202, 1973).

9.5.2 Convergence to Machine Zero

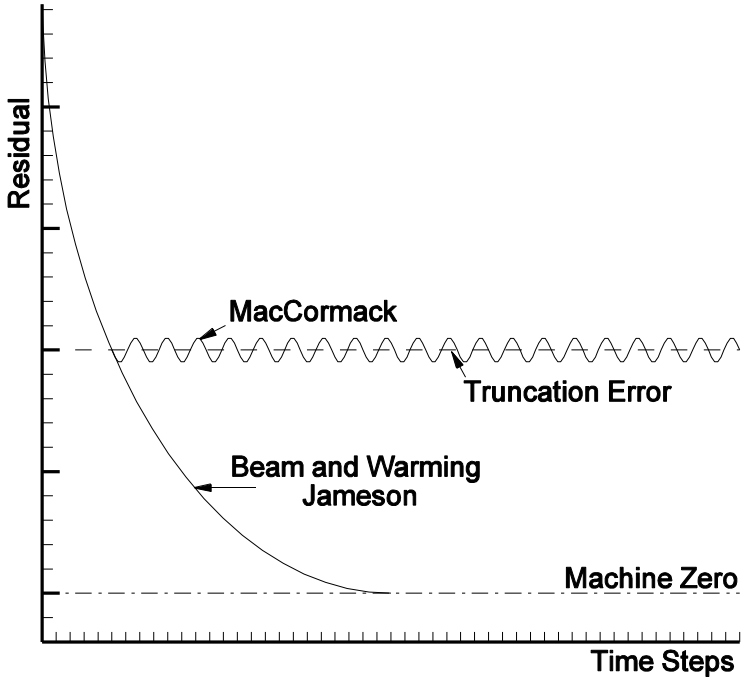

Figure 9.23 Residual convergence.

The *Beam-Warming* and *Jameson* methods use central difference approximations for spatial derivatives. Other than the disadvantage of requiring additional numerical dissipation to control "saw tooth" like error growth, these methods have the advantage of being able to converge to computer machine zero (10^{-15} on 64~bit machines). In contrast, the *MacCormack* method which alternates between forward and backward difference approximations has a built in pseudo unsteadiness and will converge at best only to the truncation error of the method.

9.6 Steger and Warming's Flux Split Method (1978)

The precise treatment of the flow physics in the classical method of characteristics was lost during the early development of finite difference procedures for general multidimensional flow calculations. Moretti reintroduced this precision in his "Lambda" scheme in the mid-1970's.

However, his method is in nonconservative form and requires special procedures at shock waves and other flow discontinuities. Steger and Warming formulated characteristics theory into conservation law form by splitting the flux vectors according to the signs of the characteristic speeds of the flow. They observed that the flux vectors for the Euler equations, F and G, equal exactly their Jacobians times the solution vector U, respectively. They rediscovered that the flux vectors of the Euler equations are homogeneous of degree **1** with respect to U (see Section 2.5).

$$F = AU \;\; and \;\; G = BU, \;\; where \;\; A = \frac{\partial F}{\partial U} \;\; and \;\; B = \frac{\partial G}{\partial U}$$

The Jacobians A and B can each be diagonalized.

$$A = S^{-1} C_A^{-1} \begin{bmatrix} u & 0 & 0 & 0 \\ 0 & u+c & 0 & 0 \\ 0 & 0 & u & 0 \\ 0 & 0 & 0 & u-c \end{bmatrix} C_A S \;\; and \;\; \mathrm{B} = S^{-1} C_B^{-1} \begin{bmatrix} v & 0 & 0 & 0 \\ 0 & v & 0 & 0 \\ 0 & 0 & v+c & 0 \\ 0 & 0 & 0 & v-c \end{bmatrix} C_B S$$

where

$$S = \begin{bmatrix} 1 & 0 & 0 & 0 \\ -u/\rho & 1/\rho & 0 & 0 \\ -v/\rho & 0 & 1/\rho & 0 \\ \alpha\beta & -u\beta & -v\beta & \beta \end{bmatrix}, \quad S^{-1} = \begin{bmatrix} 1 & 0 & 0 & 0 \\ u & \rho & 0 & 0 \\ v & 0 & \rho & 0 \\ \alpha & \rho u & \rho v & 1/\beta \end{bmatrix},$$

$$C_A = \begin{bmatrix} 1 & 0 & 0 & -1/c^2 \\ 0 & \rho c & 0 & 1 \\ 0 & 0 & 1 & 0 \\ 0 & -\rho c & 0 & 1 \end{bmatrix}, \qquad C_A^{-1} = \begin{bmatrix} 1 & \frac{1}{2c^2} & 0 & \frac{1}{2c^2} \\ 0 & \frac{1}{2\rho c} & 0 & \frac{-1}{2\rho c} \\ 0 & 0 & 1 & 0 \\ 0 & 1/2 & 0 & 1/2 \end{bmatrix},$$

$$C_B = \begin{bmatrix} 1 & 0 & 0 & -1/c^2 \\ 0 & 1 & 0 & 0 \\ 0 & 0 & \rho c & 1 \\ 0 & 0 & -\rho c & 1 \end{bmatrix}, \qquad C_B^{-1} = \begin{bmatrix} 1 & 0 & \frac{1}{2c^2} & \frac{1}{2c^2} \\ 0 & 1 & 0 & 0 \\ 0 & 0 & \frac{1}{2\rho c} & \frac{-1}{2\rho c} \\ 0 & 0 & 1/2 & 1/2 \end{bmatrix}$$

$$\text{with } \alpha = \frac{u^2+v^2}{2} \;\; and \;\; \beta = \gamma - 1$$

To give meaning to the matrices consider the following transformations

$$\delta V = \left.\frac{\partial V}{\partial U}\right|_{S} \delta U \qquad \text{and} \qquad \delta C_{h_A} = \left.\frac{\partial C_{h_A}}{\partial V}\right|_{C_A} \delta V, \quad \text{where} \quad V = \begin{bmatrix} \rho \\ u \\ v \\ p \end{bmatrix} \quad \text{and} \quad \delta C_{h_A} = \begin{bmatrix} \delta\rho - \delta p / c^2 \\ \rho c \delta u + \delta p \\ \delta v \\ -\rho c \delta u + \delta p \end{bmatrix}$$

Unlike the vector U containing the conservation variables, the vector V contains as elements the primitive or non-conserved variables. The vector δC_{h_A} contains the change in characteristic variables related to the change in primitive variables through the jacobian $C_A = \dfrac{\partial C_{h_A}}{\partial V}$, etc.

The elements of the two diagonal matrices above can be either positive or negative, indicating that characteristic information can travel in either the positive or negative x or y coordinate directions. For example, for subsonic flow moving in the x-coordinate direction the characteristic speeds u and $u+c$ are positive and $u-c$ is negative. This suggests, from both domain of dependence and numerical stability considerations, that backward difference approximations should be used for spatial derivatives for that part of the flux terms corresponding to positive characteristic speeds, and forward difference approximations for that part corresponding to negative characteristic speeds. The flux can be split as follows.

$$F_+ = A_+ U, \quad F_- = A_- U, \quad G_+ = B_+ U \quad \textit{and} \quad G_- = B_- U,$$

where $A_+ = S^{-1} C_A^{-1} \Lambda_{A_+} C_A S$, $A_- = A - A_+$ and $B_+ = S^{-1} C_B^{-1} \Lambda_{B_+} C_B S$, $B_- = B - B_+$

The matrices Λ_{A_+} and Λ_{B_+} contain the positive elements of Λ_A and Λ_B, respectively, with zeros replacing the negative elements.

An explicit Steger-Warming flux split difference equation for solving the unsteady Euler equations is

$$U_{i,j}^{n+1} = U_{i,j}^{n} - \Delta t \left(\frac{D_- \cdot}{\Delta x} F_{+_{i,j}}^{n} + \frac{D_+ \cdot}{\Delta x} F_{-_{i,j}}^{n} + \frac{D_- \cdot}{\Delta y} G_{+_{i,j}}^{n} + \frac{D_+ \cdot}{\Delta y} G_{-_{i,j}}^{n} \right)$$

9.6.1 A Numerical Difficulty Caused When an Eigenvalue Vanishes

An early difficulty was encountered when a characteristic speed passed through zero. This caused the derivatives of the split flux terms to be discontinuous, which then produced anomalies in the numerical solution. An alternative explanation is that numerical anomalies once created become trapped where eigenvalues vanish, much like flotsam and jetsam in a stagnant region of a flow. This difficulty was corrected by replacing the positive and negative characteristic speeds, $\lambda_\pm$, with the following $\lambda'_\pm$.

$$\lambda_+ = \frac{\lambda + |\lambda|}{2} \quad \text{is replaced by} \quad \lambda'_+ = \frac{\lambda + \sqrt{\lambda^2 + \varepsilon^2}}{2}$$

$$\lambda_- = \frac{\lambda - |\lambda|}{2} \quad \text{is replaced by} \quad \lambda'_- = \frac{\lambda - \sqrt{\lambda^2 + \varepsilon^2}}{2}$$

where ε is small. Bram van Leer (1981) has also contributed modifications to remove this same difficulty when characteristic speeds vanish. This change, besides removing discontinuities, increases the characteristic speed away from zero, allowing trapped anomalies a chance to move away. The overlapping non-zero values of λ_+ and λ_-, seen in the figure below, where $\lambda = 0$ also increases the dissipation of the method, which would otherwise vanish when the characteristic speed vanishes.

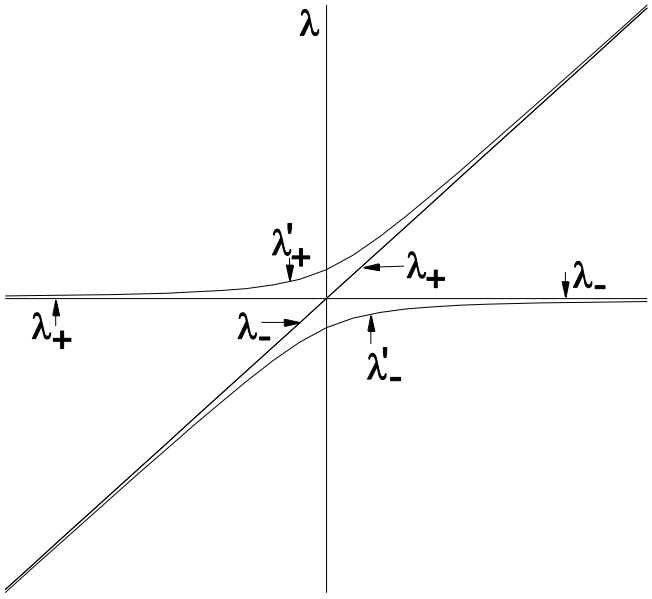

Figure 9.24 Split flux eigenvalues.

9.6.2 Exercise: Calculate the flow within the shock tube problem given in Section 9.2 using the Steger-Warming method. The numerical solution (solid symbols) using the Steger-Warming Flux Split method for the shock tube problem is compared with the exact solution for density below after 40 time steps using $\Delta t = 0.9 \left. \frac{\Delta x}{|u| + c} \right|_{\min}$. Note the beginning of instability in the solutions near the shock wave despite the CFL number being less than one. This numerical difficulty is not related solely to the vanishing eigenvalue difficulty discussed in the last section, although it may have initiated it at the shock wave. It is related to the large numerical dissipation inherent in the Steger-Warming method. Too much dissipation can also cause instability.

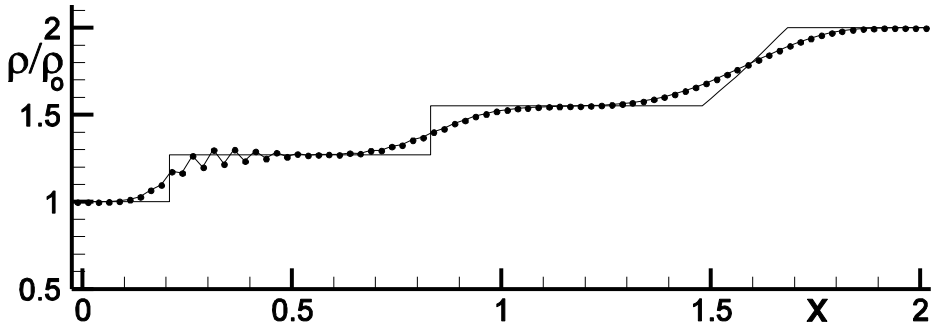

Figure 9.25 Density comparison for the Steger-Warming method (CFL=0.9)

The CFL safety factor of 0.9 was not sufficiently large to cover for the methods numerical dissipation. See, for example the mixed inviscid-viscous CFL stability criterion in Section 4.4.6. A more restrictive limit on the time step size is needed to prevent the "saw tooth" error from growing. The characteristic speed $|u|+c$ in the denominator of the stability criterion was not sufficient to account for the added numerical dissipation in the method. The calculation was repeated with an larger CFL safety factor, $\Delta t = 0.8\left.\dfrac{\Delta x}{|u|+c}\right|_{\min}$, and the results are shown below. Note the smooth solution obtained. The dissipative nature of the method severely smoothed all discontinuities.

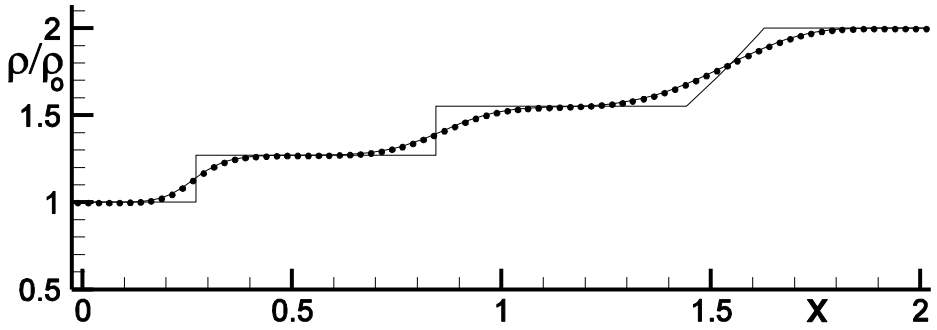

Figure 9.26 Density comparison for the Steger-Warming method (CFL=0.8)

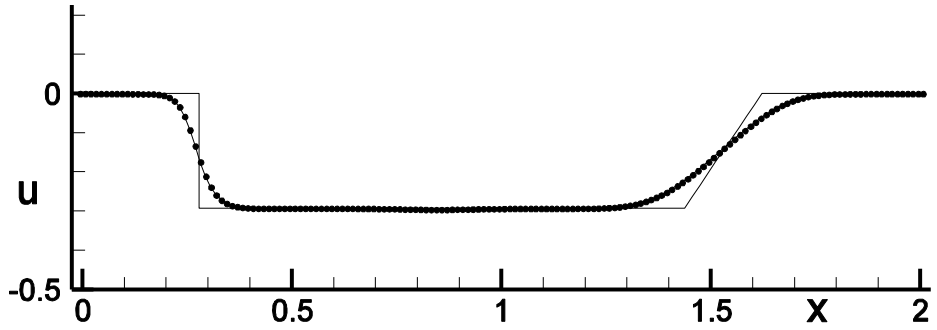

Figure 9.27 Velocity comparison for the Steger-Warming method (CFL=0.8)

9.6.3 The Dissipative Nature of the Steger-Warming Flux Split Method

The velocity distribution for the shock tube problem solution, at CFL=0.9, using the Steger-Warming method is shown below. The growth of an instability is seen near $x = 0.5$. We will try to understand this in his section.

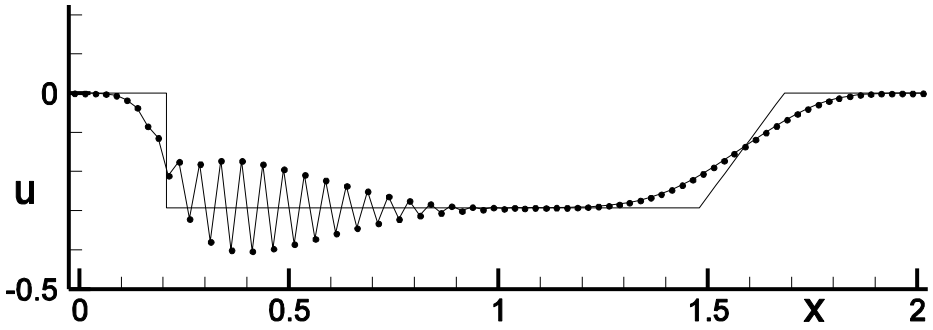

Figure 9.28 Velocity comparison for the Steger-Warming method (CFL=0.9)

The one dimensional Steger-Warming algorithm can be written as follows

$$U_i^{n+1} = U_i^n - \Delta t\left(\frac{D_-}{\Delta x}\cdot F_{+_i}^n + \frac{D_+}{\Delta x}\cdot F_{-_i}^n\right) = U_i^n - \Delta t\left(\frac{(F_{+_i}^n + F_{-_{i+1}}^n) - (F_{+_{i-1}}^n + F_{-_i}^n)}{\Delta x}\right)$$

The flux passing from mesh point "i" to mesh point "$i+1$" is

$$F_{i+1/2}^n = \begin{bmatrix} \rho u \\ \rho u^2 + p \\ (e+p)u \end{bmatrix}_{i+1/2} = F_{+_i}^n + F_{-_{i+1}}^n = A_{+_i}^n U_i^n + A_{-_{i+1}}^n U_{i+1}^n$$

For the one dimensional Steger-Warming algorithm

$$AU = S^{-1}C^{-1}\Lambda CSU = S^{-1}C^{-1}\Lambda C\begin{bmatrix} 1 & 0 & 0 \\ -\dfrac{u}{\rho} & \dfrac{1}{\rho} & 0 \\ \alpha\beta & -u\beta & \beta \end{bmatrix}\begin{bmatrix} \rho \\ \rho u \\ e \end{bmatrix} = S^{-1}C^{-1}\Lambda\begin{bmatrix} 1 & 0 & -1/c^2 \\ 0 & \rho c & 1 \\ 0 & -\rho c & 1 \end{bmatrix}\begin{bmatrix} \rho \\ 0 \\ p \end{bmatrix}$$

$$= S^{-1}C^{-1}\begin{bmatrix} u & 0 & 0 \\ 0 & u+c & 0 \\ 0 & 0 & u-c \end{bmatrix}\begin{bmatrix} \rho - p/c^2 \\ p \\ p \end{bmatrix}$$

The characteristic speeds are $u,\ u+c$ *and* $u-c$. For the shock tube problem $u \le 0$, $u+c > 0$ and $u-c < 0$ throughout the flow field. This implies that the flux carried by the first and third

characteristic speeds will be forward differenced and the second will be backward differenced by the algorithm. For the first characteristic speed

$$F_u = S_{i+1}^{-1} C_{i+1}^{-1} \begin{bmatrix} u_{i+1} & 0 & 0 \\ 0 & 0 & 0 \\ 0 & 0 & 0 \end{bmatrix} \begin{bmatrix} \rho_{i+1} - \dfrac{p_{i+1}}{c_{i+1}^2} \\ p_{i+1} \\ p_{i+1} \end{bmatrix} = S_{i+1}^{-1} \begin{bmatrix} 1 & \dfrac{1}{2c_{i+1}^2} & \dfrac{1}{2c_{i+1}^2} \\ 0 & \dfrac{1}{2\rho_{i+1}c_{i+1}} & \dfrac{-1}{2\rho_{i+1}c_{i+1}} \\ 0 & 1/2 & 1/2 \end{bmatrix} \begin{bmatrix} u_{i+1}(\rho_{i+1} - \dfrac{p_{i+1}}{c_{i+1}^2}) \\ 0 \\ 0 \end{bmatrix}$$

$$= u_{i+1}(\rho_{i+1} - \frac{p_{i+1}}{c_{i+1}^2}) \begin{bmatrix} 1 & 0 & 0 \\ u_{i+1} & \rho_{i+1} & 0 \\ \alpha_{i+1} & \rho_{i+1}u_{i+1} & 1/\beta \end{bmatrix} \begin{bmatrix} 1 \\ 0 \\ 0 \end{bmatrix} = u_{i+1}(\rho_{i+1} - \frac{p_{i+1}}{c_{i+1}^2}) \begin{bmatrix} 1 \\ u_{i+1} \\ \alpha_{i+1} \end{bmatrix}$$

Similarly, for the second and third characteristic speeds

$$F_{u+c} = (u_i + c_i)\frac{p_i}{2c_i^2} \begin{bmatrix} 1 \\ u_i + c_i \\ \alpha_i + u_i c_i + \dfrac{c_i^2}{\beta} \end{bmatrix} \text{ and } F_{u-c} = (u_{i+1} - c_{i+1})\frac{p_{i+1}}{2c_{i+1}^2} \begin{bmatrix} 1 \\ u_{i+1} - c_{i+1} \\ \alpha_{i+1} - u_{i+1}c_{i+1} + \dfrac{c_{i+1}^2}{\beta} \end{bmatrix}$$

Finally, the total flux is

$$F_{i+1/2} = \begin{bmatrix} u_{i+1}(\rho_{i+1} - \dfrac{p_{i+1}}{c_{i+1}^2}) + (u_i + c_i)\dfrac{p_i}{2c_i^2} + (u_{i+1} - c_{i+1})\dfrac{p_{i+1}}{2c_{i+1}^2} \\ u_{i+1}(\rho_{i+1} - \dfrac{p_{i+1}}{c_{i+1}^2})u_{i+1} + (u_i + c_i)\dfrac{p_i}{2c_i^2}(u_i + c_i) + (u_{i+1} - c_{i+1})\dfrac{p_{i+1}}{2c_{i+1}^2}(u_{i+1} - c_{i+1}) \\ u_{i+1}(\rho_{i+1} - \dfrac{p_{i+1}}{c_{i+1}^2})\alpha_{i+1} + (u_i + c_i)\dfrac{p_i}{2c_i^2}(\alpha_i + u_i c_i + \dfrac{c_i^2}{\beta}) + (u_{i+1} - c_{i+1})\dfrac{p_{i+1}}{2c_{i+1}^2}(\alpha_{i+1} - u_{i+1}c_{i+1} + \dfrac{c_{i+1}^2}{\beta}) \end{bmatrix}$$

which can be rearranged as

$$F_{i+1/2} = \begin{bmatrix} u_{i+1}\rho_{i+1} + \dfrac{u_i + c_i}{2\gamma}\rho_i - \dfrac{u_{i+1} + c_{i+1}}{2\gamma}\rho_{i+1} \\ \rho_{i+1}u_{i+1}^2 + (1 + \dfrac{u_i}{c_i})\dfrac{p_i}{2} + (1 - \dfrac{u_{i+1}}{c_{i+1}})\dfrac{p_{i+1}}{2} + \dfrac{u_i + c_i}{2\gamma}\rho_i u_i - \dfrac{u_{i+1} + c_{i+1}}{2\gamma}\rho_{i+1}u_{i+1} \\ (e_{i+1} + p_{i+1})u_{i+1} + (1 + \dfrac{u_i}{c_i})\dfrac{p_i u_i}{2} + (1 - \dfrac{u_{i+1}}{c_{i+1}})\dfrac{p_{i+1}u_{i+1}}{2} + \dfrac{u_i + c_i}{2\gamma}(e_i + p_i) - \dfrac{u_{i+1} + c_{i+1}}{2\gamma}(e_{i+1} + p_{i+1}) \end{bmatrix}$$

We can interpret the flux as follows, using the momentum flux as an example

$$(\rho u^2 + p)_{i+1/2} \approx \rho_{i+1} u_{i+1}^2 + (1+\frac{u_i}{c_i})\frac{p_i}{2} + (1-\frac{u_{i+1}}{c_{i+1}})\frac{p_{i+1}}{2} + \frac{u_i + c_i}{2\gamma}\rho_i u_i - \frac{u_{i+1} + c_{i+1}}{2\gamma}\rho_{i+1} u_{i+1}$$

First, $(\rho u^2)_{i+1/2} \approx \rho_{i+1} u_{i+1}^2$ and $p_{i+1/2} \approx (1+\frac{u_i}{c_i})\frac{p_i}{2} + (1-\frac{u_{i+1}}{c_{i+1}})\frac{p_{i+1}}{2}$

Note that pressure is approximated as a weighted average, using the local Mach number to add more weight to the upstream, which is to the left for the negative values of velocity. The final set of terms represents a viscous mixing introduced by the Steger-Warming method.

$\Delta x \frac{\partial \nu(\rho u)}{\partial x} \approx \frac{u_i + c_i}{2\gamma}\rho_i u_i - \frac{u_{i+1} + c_{i+1}}{2\gamma}\rho_{i+1} u_{i+1}$, with coefficient of viscosity $\nu \approx \Delta x \frac{u+c}{2\gamma}$.

This indicates that according to Section 4.4.6 the Steger-Warming method is stable if

$$\Delta t \le \frac{\Delta x}{|u| + c + 2\nu/\Delta x}$$

The curves for $\Delta t = 0.9\frac{\Delta x}{|u|+c}$, $\Delta t = 0.8\frac{\Delta x}{|u|+c}$, $\Delta t = 0.7\frac{\Delta x}{|u|+c}$ and $\Delta t = \frac{\Delta x}{|u| + c + 2\nu/\Delta x}$ versus x are shown below using the solution procedure as shown in Figures 9.25 - 9.28.

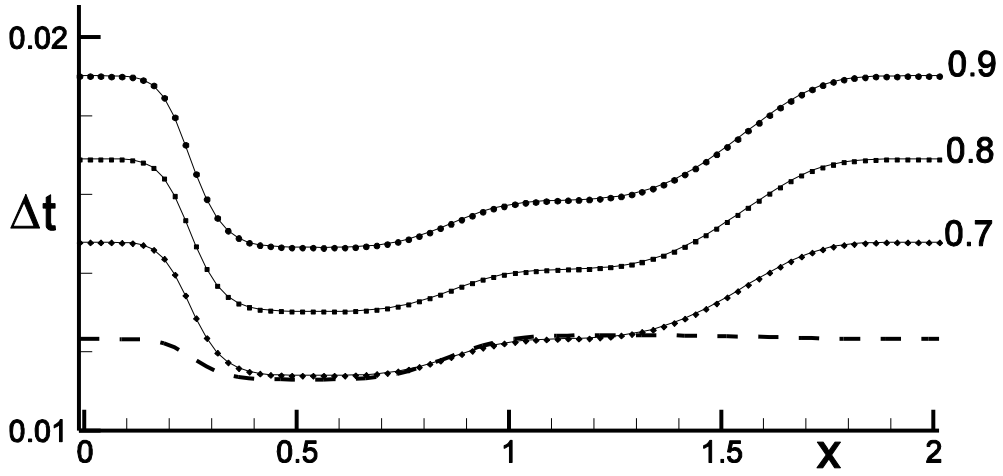

Figure 9.29 Time step size criteria vs. x

The time step size that should be used is the minimum value for each curve over the mesh at each time step. The heavy dashed curve above, $\Delta t = \frac{\Delta x}{|u| + c + 2\nu/\Delta x}$ vs. x, indicates that the

Steger-Warming method would be stable for this problem if the CFL number $\frac{(|u|+c)\Delta t}{\Delta x}$ was less than 0.7. However, 0.8 sufficed as shown above.

9.7 Conservative Difference Equations in Generic Form

Algorithms for solving the equations of fluid dynamics are usually presented in a generic form with the fluxes evaluated at the interfaces between mesh points. A general example is given below.

$$\left\{I+\Delta t(\cdots)\right\}\delta U_{i,j}^{n+1}=-\Delta t\left(\frac{F_{i+1/2,j}^{n}-F_{i-1/2,j}^{n}}{\Delta x}+\frac{G_{i,j+1/2}^{n}-G_{i,j-1/2}^{n}}{\Delta y}\right)$$

In terms of the Steger-Warming split fluxes $F_{i+1/2,j}^{n}=F_{+_{i,j}}^{n}+F_{-_{i+1,j}}^{n}=A_{+_{i,j}}^{n}U_{i,j}^{n}+A_{-_{i+1,j}}^{n}U_{i+1,j}^{n}$

Note that the flux is defined halfway between mesh points (i,j) and $(i+1,j)$. The positive traveling part of the flux comes to this surface from the left and the negative traveling part of the flux from the right.

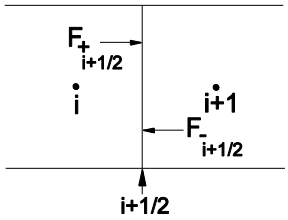

Figure 9.30 Flux surface $\xi=i+1/2$

Similarly, $G_{i,j+1/2}^{n}=G_{+_{i,j}}^{n}+G_{-_{i,j+1}}^{n}=B_{+_{i,j}}^{n}U_{i,j}^{n}+B_{-_{i,j+1}}^{n}U_{i,j+1}^{n}$

Note that the subscripts on the split Jacobians for the *Steger-Warming* method, A_{+}^{n}, A_{-}^{n}, B_{+}^{n} and B_{-}^{n}, exactly match, and use the data from, the state vector U that they multiply.

9.8 The Modified Steger-Warming Method

9.8.1 Version (1) - Splitting the Flux Vector via the State Vector

The Steger-Warming Method was originally developed to solve the Euler equations. It is fairly dissipative and should not be used as is for solving the Navier-Stokes equations where true dissipative phenomena are to be resolved. The following modification greatly reduces the usually unneeded numerical dissipation found in the Steger-Warming method. In terms of the "generic" flux presented in the last section

$$F_{i+1/2,j}^{n}=F_{+_{i+1/2,j}}^{n}+F_{-_{i+1/2,j}}^{n}=\overline{A}_{+_{i+1/2,j}}^{n}U_{i,j}^{n}+\overline{A}_{-_{i+1/2,j}}^{n}U_{i+1,j}^{n}$$

Similarly

$$G_{i,j+1/2}^{n}=G_{+_{i,j+1/2}}^{n}+G_{-_{i,j+1/2}}^{n}=\overline{B}_{+_{i,j+1/2}}^{n}U_{i,j}^{n}+\overline{B}_{-_{i,j+1/2}}^{n}U_{i,j+1}^{n}$$

Note that now the subscripts on the split Jacobians for the Modified Steger-Warming method, $\overline{A}_{+}^{n}$, $\overline{A}_{-}^{n}$, $\overline{B}_{+}^{n}$ and $\overline{B}_{-}^{n}$, no longer match the subscripts on the state vector U that they multiply.

These Jacobians for the Modified Steger-Warming method, are evaluated using "arithmetically" averaged data from the nearest grid points to the surface at which the flux is to be approximated. For example, the elements of

$$\overline{A}^n_{+_{i+1/2,j}} \text{ uses data from } \overline{U}^n_{i+1/2,j} = \frac{U^n_{i,j} + U^n_{i+1,j}}{2}, \quad \overline{B}^n_{+_{i,j+1/2}} \text{ uses data from } \overline{U}^n_{i,j+1/2} = \frac{U^n_{i,j} + U^n_{i,j+1}}{2}$$

The conservative state vector U is averaged as above to determine the data needed to evaluate the split Jacobians. The nonconservative state vector $V = [\rho, u, v, p]^T$ could also be used. The best choice will depend on the flow situation and which flow variables have the least variation. For inviscid flow, containing shock waves, using the conservative U may be better. However, for viscous flow within a boundary layer, where the pressure is fairly constant, the nonconservative V may be better. In Section 9.9, presenting the Roe method, a different set of flow variables are chosen, including a "geometric" average for density.

9.8.1.1 Correction for the Modified-Steger-Warming Method

The Modified-Steger-Warming flux is significantly less dissipative than the unmodified Steger-Warming flux. This can be demonstrated by a similar analysis to that used in Section 9.6.3. In certain instances, such as at the foot of a shock wave, there may be insufficient numerical dissipation in the modified method to prevent negative pressures from occurring. This can be corrected by blending some of the unmodified flux with the modified flux in strong pressure gradient regions. For example, for the "x" flow direction, let $pg_{i+1/2}$, for pressure gradient, be defined by

$$pg_{i+1/2} = \frac{p_{i+1} - p_i}{\min\{p_i, p_{i+1}\}},$$

and weight $wt_{i+1/2}$ be defined by

$$wt_{i+1/2} = \frac{1}{1 + pg^2_{i+1/2}}$$

Note that $0 \le wt_{i+1/2} \le 1$. The blended split flux is then given by

$$F_{i+1/2} = wt_{i+1/2} F^{(M-S-W)}_{i+1/2} + (1 - wt_{i+1/2}) F^{(S-W)}_{i+1/2}$$

The modified and unmodified Steger-Warming methods differ in only how the data used in their Jacobians are defined. Therefore, an easy way to introduce the blending described above is to the blend the variables used to determine the Jacobians. The Jacobians defined in the beginning of Section 9.6 depend upon the variables ρ, u, v and c. Actually, the dependence upon ρ can be avoided, which will be discussed at a later time. If we take the variable c as an example, then we can redefine a blended c^+, to be used in the matrices defining A_+, as follows.

$$c^{+}_{i+1/2} = wt_{i+1/2}\frac{c_i + c_{i+1}}{2} + \left(1 - wt_{i+1/2}\right)c_i$$

and, similarly for a blended c^{-}, to be used in the matrices defining A_{-},

$$c^{-}_{i+1/2} = wt_{i+1/2}\frac{c_i + c_{i+1}}{2} + \left(1 - wt_{i+1/2}\right)c_{i+1}$$

The other variables are similarly defined.

9.8.1.2 Exercise: Calculate the flow within the shock tube problem given in Section 9.2 using the Modified-Steger-Warming method. The numerical solution (solid symbols) using the Modified Steger-Warming method for the shock tube problem is compared with the exact solution for density below after 40 time steps using $\Delta t = 0.9\left.\frac{\Delta x}{|u| + c}\right|_{\min}$. These results did not need the corrections discussed in Section 9.8.1.1.

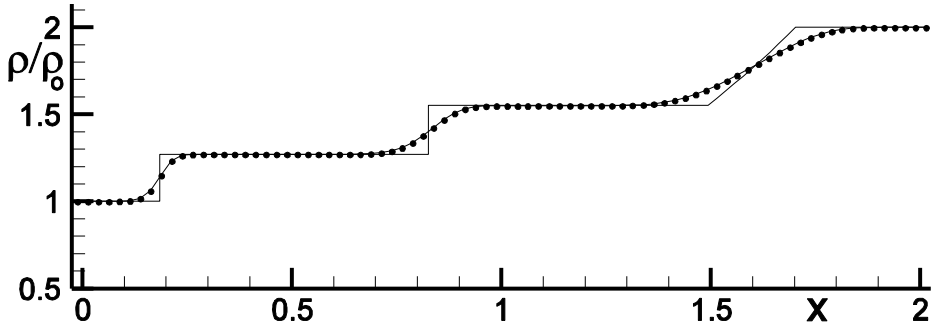

Figure 9.31 Density comparison for the Modified Steger-Warming method (CFL=0.9), Version (1), with no correction

9.8.2 Version (2) - Splitting the Flux Vector via the Flux Vector Itself

Earlier in Section 9.6 we used for the Euler equations the relations

$$F = AU \;\; and \;\; G = BU, \;\; where \;\; A = \frac{\partial F}{\partial U} \;\; and \;\; B = \frac{\partial G}{\partial U}$$

We can turn these inside out as follows, assuming for the moment that the inverses exist, (i.e., the eigenvalues of A and B do not vanish).

$$U = A^{-1}F \;\; and \;\; U = B^{-1}G, \text{ where } A^{-1} = S^{-1}C_A^{-1}\Lambda_A^{-1}C_A S \text{ and } B^{-1} = S^{-1}C_B^{-1}\Lambda_B^{-1}C_B S$$

Therefore, we can split the fluxes F and G directly as follows

$$F_{\pm} = S^{-1}C_A^{-1}\Lambda_{A_{\pm}}\Lambda_A^{-1}C_A S\,F = S^{-1}C_A^{-1}D_{A_{\pm}}C_A S\,F = \mathcal{A}_{\pm}F$$

and

$$G_{\pm} = S^{-1}C_B^{-1}\Lambda_{B_{\pm}}\Lambda_B^{-1}C_B S\,G = S^{-1}C_B^{-1}D_{B_{\pm}}C_B S\,G = \mathcal{B}_{\pm}G$$

where the diagonal matrices $D_{A_{\pm}}$ and $D_{B_{\pm}}$ have "ones" or "zeros" as elements. For example, D_{A_+} has "ones" where Λ_{A_+} has non-zero elements and $D_{A_-} = I - D_{A_+}$. This approach has the benefit of partitioning the conservative flux vectors themselves, which, for example, unlike the state vectors, are often continuous across discontinuities in the flow (see Section 2.4). Notice the new matrices $\mathcal{A}_{\pm}$ and $\mathcal{B}_{\pm}$ defined above.

In terms of the generic flux vectors

$$F^n_{i+1/2,j} = \mathcal{A}^n_{+_{i+1/2,j}} F^n_{i,j} + \mathcal{A}^n_{-_{i+1/2,j}} F^n_{i+1,j}$$

and

$$G^n_{i,j+1/2} = \mathcal{B}^n_{+_{i,j+1/2}} G^n_{i,j} + \mathcal{B}^n_{-_{i,j+1/2}} G^n_{i,j+1}$$

9.8.2.1 Exercise: Calculate the flow within the shock tube problem given in Section 9.2 using the Modified-Steger-Warming method with the *flux vector split directly*. The numerical solution (solid symbols) using the Modified Steger-Warming method, Version (2), for the shock tube problem is compared with the exact solution for density below after 40 time steps using $\Delta t = 0.9\left.\dfrac{\Delta x}{|u|+c}\right|_{\min}$. Again, no correction was required.

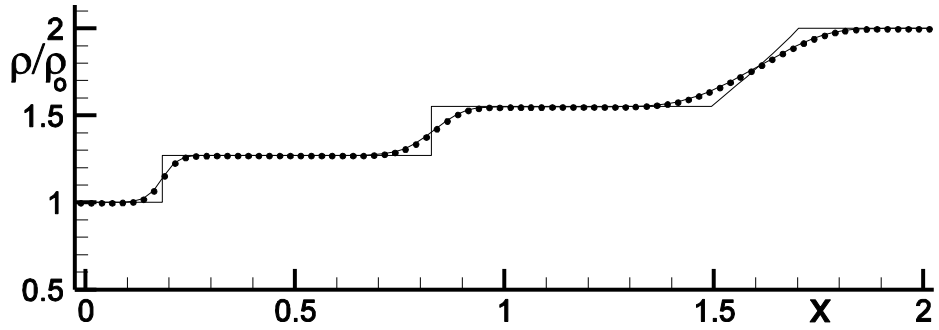

Figure 9.32 Density comparison for the Modified Steger-Warming method (CFL=0.9) with direct splitting of flux vector, Version (2).

9.9 The Roe Flux Difference Vector Splitting Method

There are three important distinctions that characterize Roe's Method.

1) The split Jacobian matrices use averaged data chosen to approximately solve the Riemann problem.
2) The method actually splits the "flux difference" vector in contrast to the Steger-Warming and Modified-Steger-Warming methods that split only the flux vector itself.
3) The method returns the exact solution whenever only a single discontinuity is present.

The Roe Method is widely chosen today because of the above properties. They will be discussed in turn, where for simplicity the subscript index j or i will be suppressed when not essential. First, the elements of the Jacobian matrix $A_{i+1/2}$ are chosen to satisfy the following equation.

$$F_{i+1} - F_i = \hat{A}_{i+1/2}\left(U_{i+1} - U_i\right)$$

This equation relates two arbitrary fluid states, state "i" and state "$i+1$", with the Jacobian $A_{i+1/2}$. They may be two states on either side of a shock wave or contact discontinuity. This equation represents the so called Riemann problem.

The elements of $A_{i+1/2}$, for the 2-D Euler equations, are determined from

$$\hat{\rho}_{i+1/2} = \rho_i^{1/2}\rho_{i+1}^{1/2}$$

$$u_{i+1/2} = \frac{\rho_i^{1/2}u_i + \rho_{i+1}^{1/2}u_{i+1}}{\rho_i^{1/2} + \rho_{i+1}^{1/2}}$$

$$\hat{v}_{i+1/2} = \frac{\rho_i^{1/2}v_i + \rho_{i+1}^{1/2}v_{i+1}}{\rho_i^{1/2} + \rho_{i+1}^{1/2}}$$

$$h_{i+1/2} = \frac{\rho_i^{1/2}\dfrac{e_i + p_i}{\rho_i} + \rho_{i+1}^{1/2}\dfrac{e_{i+1} + p_{i+1}}{\rho_{i+1}}}{\rho_i^{1/2} + \rho_{i+1}^{1/2}}$$

***Exercise*:** Show that the equation $F_{i+1} - F_i = \hat{A}_{i+1/2}\left(U_{i+1} - U_i\right)$, which relates states "$i$" and "$i+1$", is satisfied for the Euler equations using the Roe averaged variables for $A_{i+1/2}$.

The Roe flux, in generic terms, is defined by

$$F_{i+1/2} = \frac{F_i + F_{i+1}}{2} - \frac{1}{2}\left|\hat{A}_{i+1/2}\right|\left(U_{i+1} - U_i\right)$$

$$\text{where we define } \left|A\right| = A_+ - A_-$$

With the above Roe flux definition, it can be shown that

$$F_{1+1/2} - F_{i-1/2} = \left(F_{i+1} - F_i\right)_- + \left(F_i - F_{i-1}\right)_+$$

$$\text{where } \left(F_{i+1} - F_i\right)_- = \hat{A}_{-\,i+1/2}\left(U_{i+1} - U_i\right)$$

$$\text{and } \left(F_i - F_{i-1}\right)_+ = \hat{A}_{+\,i-1/2}\left(U_i - U_{i-1}\right)$$

Therefore, as seen above, the Roe method splits the flux difference vector.

If the flux difference vector is zero, there will be zero split flux. This may seem to be a subtle point, but for shocks it is significant. Consider, for example, a steady shock wave in one dimension (see the equations given in Section 2.4, either the stationary shock relation, with shock speed $w=0$, or the oblique shock wave relations with $\theta=\pi/2$). The flux vector F is constant while the state vector U jumps. The Roe method can capture this shock exactly - with no "wiggles".

9.9.1 The Entropy Correction for the Roe Method

The method is a bit, however, "shock happy" and will often place sharp jumps when none would be physically expected, such as in expansion regions through Mach one. An entropy correction can be added to avoid this situation as follows. Let $\lambda_{i+1/2}$ be an eigenvalue of $A_{i+1/2}$.

$$\lambda_{i+1/2} = u_{i+1/2},\ u_{i+1/2}+\hat{c}_{i+1/2} \text{ or } u_{i+1/2}-\hat{c}_{i+1/2}$$

$$\text{where } \hat{c}_{i+1/2} = \sqrt{(\gamma-1)\left(h_{i+1/2}-\frac{1}{2}\left(u^2_{i+1/2}+\hat{v}^2_{i+1/2}\right)\right)}.$$

Let λ_i and λ_{i+1} (without the hat symbols) be the values of this eigenvalue at point i and $i+1$ and $\varepsilon_{i+1/2}$ be defined as follows.

$$\varepsilon_{i+1/2} = \sigma_0 \max\left\{0,\ \lambda_{i+1/2}-\lambda_i,\ \lambda_{i+1}-\lambda_{i+1/2}\right\},$$

where σ_0 is a constant, usually equal to 1, but may need to be increased for some flow problems.

Then

$$\textit{if} \quad \left|\lambda_{i+1/2}\right| < \varepsilon_{i+1/2} \quad \textit{then} \quad \lambda_{i+1/2} \leftarrow \frac{1}{2}\left(\frac{\lambda^2_{i+1/2}}{\varepsilon_{i+1/2}}+\varepsilon_{i+1/2}\right)$$

Note that $\varepsilon_{i+1/2}$ is always non-negative and is greater than zero only when λ is an increasing function of i (or x), which corresponds to an expansion region.

The numerical solution (solid symbols) using the Roe method for the shock tube problem of Section 9.2 is compared with the exact solution for density below after 40 time steps using $\Delta t = 0.9\left.\dfrac{\Delta x}{|u|+c}\right|_{\min}$. No entropy correction was needed for this flow problem

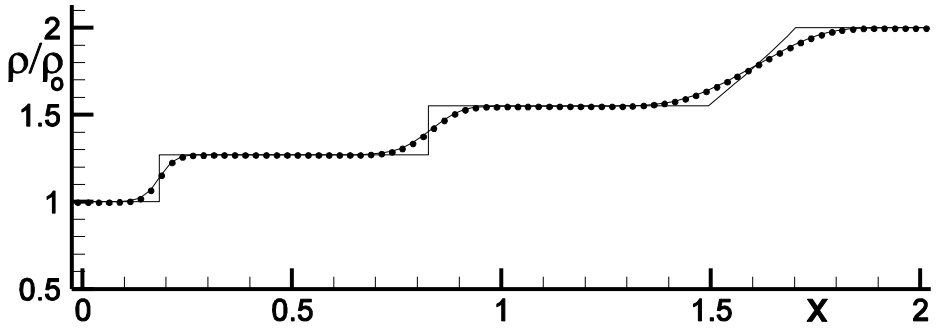

Figure 9.33 Density comparison for the Roe method, with no entropy correction, (CFL=0.9)

These results look very similar to those for the Modified Steger-Warming methods shown in Figures 9.31 and 9.32. The sharpness of the shock did not improve for this problem with the shock wave moving through the mesh.

9.9.2 The Stationary Shock Tube Problem and the Roe Method

The figure below corresponds to a stationary shock calculation by the Roe method. It is essentially the same shock tube problem as before, but now computed in a frame in which the shock wave is stationary. This is achieved by subtracting the negative shock speed from the previous flow speed, initially at rest, so that the flow now moves from left to right. The position of the diaphragm has also been moved forward. Notice the improved shock wave resolution. The contact discontinuity and rarefaction fan region remain nearly as before.

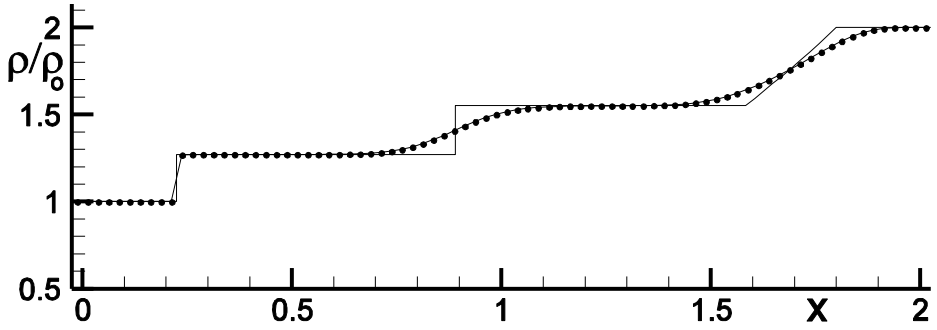

Figure 9.34 Density comparison for the Roe method, with no entropy correction, stationary shock wave, (CFL=0.9, 35 time steps)

9.10 Comparison of the Split Fluxes in Generic Form

1) The Steger-Warming split vector flux is given by

$$F_{i+1/2}^{(S-W)} = A_{+_i} U_i + A_{-_{i+1}} U_{i+1}$$

2) The Modified-Steger-Warming split vector flux is given by
Version (1), using state vector U

$$F_{i+1/2}^{(M-S-W-I)} = \overline{A}_{+_{i+1/2}} U_i + \overline{A}_{-_{i+1/2}} U_{i+1}$$

Version (2), using flux vector directly

$$F_{i+1/2}^{(M-S-W-II)} = \bar{\mathcal{A}}_{+_{i+1/2}} F_i + \bar{\mathcal{A}}_{-_{i+1/2}} F_{i+1}$$

3) The Roe split difference vector flux is given by

$$F_{i+1/2}^{(Roe)} = \frac{F_i + F_{i+1}}{2} - \frac{1}{2}\left|\hat{A}_{i+1/2}\right|\left(U_{i+1} - U_i\right)$$

The results shown earlier for the Modified Steger-Warming method, Version (1), in Figure 9.31 did not use the correction of Section 9.8.1.1. The results using both the corrected and uncorrected Modified Steger-Warming methods, Version (1), for the stationary shock problem (see Section 9.9.2) are shown in Figures 9.35 and 9.36. Compare the severe under and overshoot at the shock wave in the results using Modified Steger-Warming method, Version (1), with no correction with those below with the correction. The shock resolution shown here is comparable to that for the Roe method. The blending of the pure Steger-Warming method eliminated the under and overshoots.

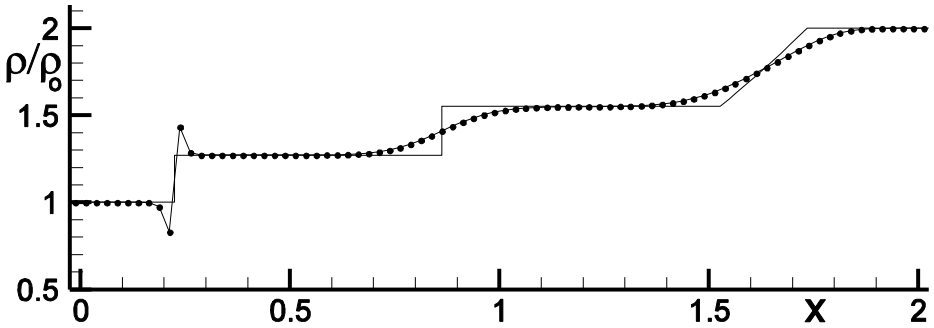

Figure 9.35 Density comparison for the Modified Steger-Warming method, Version (1), with no correction, stationary shock wave, (CFL=0.9, 35 time steps)

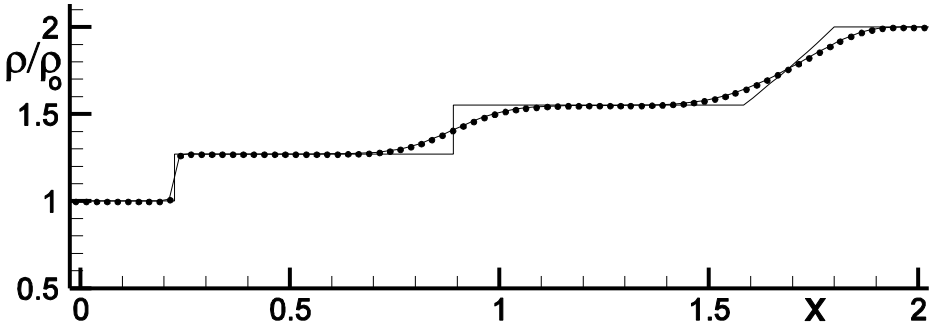

Figure 9.36 Density comparison for the Modified Steger-Warming method, Version (1), with correction, stationary shock wave, (CFL=0.9, 35 time steps)

The results using Modified Steger-Warming method, Version (2), for the stationary shock problem are shown below. No corrections were needed. Version (2) is therefore preferred.

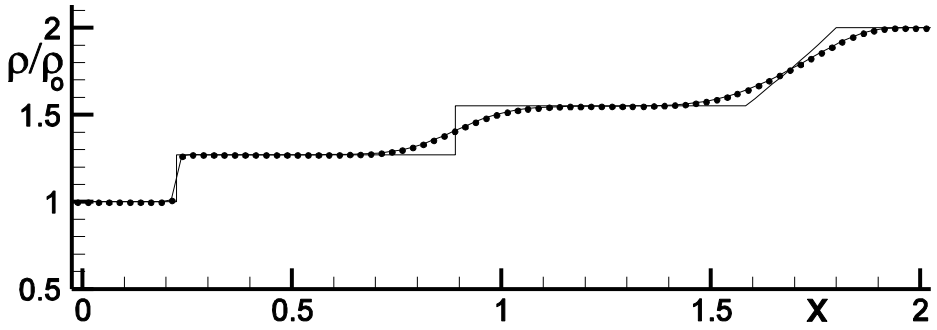

Figure 9.37 Density comparison for the Modified Steger-Warming method, Version (2), no corrections were needed, stationary shock wave, (CFL=0.9, 35 time steps)

The "captured" shock waves are very good for both the Roe and Modified-Steger-Warming methods as long as the shock waves are stationary. Moving shock waves, as well as contact discontinuities and rarefaction waves, were not so well resolved. However, the presented Modified Steger-Warming and Roe methods are only first order accurate. Resolution can be expected to improve for their second and higher order versions.

9.11 Extensions to Higher Order for the Flux Split Algorithms

The flux split methods just presented are first order accurate spatially. They can be extended to higher order accuracy by including more mesh points in the evaluation of the spatial flux terms. We will rewrite the split fluxes given in Section 9.9 in terms of U_L and U_R, the left and right values, instead of U_i and U_{i+1}. These left and right state vectors will be determined at mesh surface $i+1/2$ to a higher order accuracy using variable extrapolation. This procedure is known as Van Leer's MUSCL approach (a name derived from Monotone Upstream –centered Schemes for Conservation Laws).

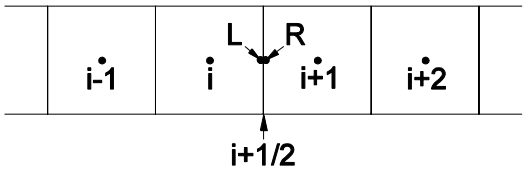

Figure 9.38 Points **L** and **R** collocated at surface $\xi = i+1/2$

The Steger-Warming split vector flux is given by

$$F_{i+1/2}^{(S-W)} = A_{+_L} U_L + A_{-_R} U_R$$

The Modified-Steger-Warming split vector flux is given by

Version (1), using state vector U

$$F_{i+1/2}^{(M-S-W-I)} = \overline{A}_{+_{i+1/2}} U_L + \overline{A}_{-_{i+1/2}} U_R$$

Version (2), using flux vector directly

$$F_{i+1/2}^{(M-S-W-II)} = \bar{\mathcal{A}}_{+_{i+1/2}} F_L + \bar{\mathcal{A}}_{-_{i+1/2}} F_R$$

The Roe split difference vector flux is given by

$$F_{i+1/2}^{(Roe)} = \frac{F_L + F_R}{2} - \frac{1}{2}\left|\hat{A}_{i+1/2}\right|\left(U_R - U_L\right)$$

The split Jacobians are evaluated also using the state vectors U_L and U_R in the same way as they previously used U_i and U_{i+1}.

9.11.1 Example, Higher Order Approximation for the Wave Equation

For the simple wave equation $\frac{\partial u}{\partial t} = -c\frac{\partial u}{\partial x}$, where c is a constant, either positive or negative, consider the flux is given by

$$F_{i+1/2} = \frac{1}{2}\left(c + |c|\right)u_L + \frac{1}{2}\left(c - |c|\right)u_R$$

If $u_L = u_i$ and $u_R = u_{i+1}$ the spatial derivative will be approximated to first order accuracy. For example, if $c > 0$ then $F_{i+1/2} = cu_i$ and, using Taylor series expansion about point i, the spatial derivative approximation becomes

$$\frac{F_{i+1/2} - F_{i-1/2}}{\Delta x} = c\frac{u_i - u_{i-1}}{\Delta x} = \frac{c}{\Delta x}\left(\cancel{u_i} - \left(\cancel{u_i} - \Delta x\frac{\partial u}{\partial x} + \frac{\Delta x^2}{2!}\frac{\partial^2 u}{\partial x^2} - \frac{\Delta x^3}{3!}\frac{\partial^3 u}{\partial x^3}\cdots\right)\right)$$

or

$$\frac{F_{i+1/2} - F_{i-1/2}}{\Delta x} = c\frac{u_i - u_{i-1}}{\Delta x} = c\left(\frac{\partial u}{\partial x} \underbrace{- \frac{\Delta x}{2!}\frac{\partial^2 u}{\partial x^2} + \frac{\Delta x^2}{3!}\frac{\partial^3 u}{\partial x^3} - \frac{\Delta x^3}{4!}\frac{\partial^4 u}{\partial x^4}\cdots}_{truncation\ \ error}\right)$$

The leading term of the truncation error, $-\frac{\Delta x}{2!}\frac{\partial^2 u}{\partial x^2}$, of first order accuracy, can be knocked out if the flux is approximated instead by $F_{i+1/2} = c\left(u_i + \frac{1}{2}(u_i - u_{i-1})\right)$, where $u_L = u_i + \frac{1}{2}(u_i - u_{i-1})$. Then, again using Taylor series expansion,

$$\frac{F_{i+1/2} - F_{i-1/2}}{\Delta x} = c\frac{u_i + \frac{1}{2}(u_i - u_{i-1}) - u_{i-1} - \frac{1}{2}(u_{i-1} - u_{i-2})}{\Delta x} = c\left(\frac{u_i - u_{i-1}}{\Delta x} + \frac{1}{2\Delta x}(u_i - 2u_{i-1} + u_{i-2})\right)$$

$$= c\left(\frac{\partial u}{\partial x} - \cancel{\frac{\Delta x}{2!}\frac{\partial^2 u}{\partial x^2}} + \frac{\Delta x^2}{3!}\frac{\partial^3 u}{\partial x^3} - \frac{\Delta x^3}{4!}\frac{\partial^4 u}{\partial x^4}\cdots \right) + c\left(\cancel{\frac{\Delta x}{2!}\frac{\partial^2 u}{\partial x^2}} - \frac{\Delta x^2}{2!}\frac{\partial^3 u}{\partial x^3} + \frac{7\Delta x^3}{4!}\frac{\partial^4 u}{\partial x^4}\cdots \right)$$

$$= c\left(\frac{\partial u}{\partial x} - \frac{2\Delta x^2}{3!}\frac{\partial^3 u}{\partial x^3} + \frac{\Delta x^3}{4!}\frac{\partial^4 u}{\partial x^4}\cdots \right)$$

The above approximation to the spatial derivative is now second order accurate. If instead the flux is approximated by $F_{i+1/2} = c\left(u_i + \frac{1}{2}(u_i - u_{i-1}) + \frac{1}{3}(u_{i+1} - 2u_i + u_{i-1}) \right)$ the above truncation error term, $-\frac{2\Delta x^2}{3!}\frac{\partial^3 u}{\partial x^3}$, can also be eliminated, yielding

$$\frac{F_{i+1/2} - F_{i-1/2}}{\Delta x} = \frac{\partial u}{\partial x} + 2\frac{\Delta x^3}{4!}\frac{\partial^4 u}{\partial x^4} + \cdots$$

The above three approximations for u_L and u_R for the simple wave equation are shown in the table below.

Method	u_L	u_R
First order upwind	u_i	u_{i+1}
Second order upwind	$\frac{1}{2}(3u_i - u_{i-1})$	$\frac{1}{2}(3u_{i+1} - u_{i+2})$
Third order upwind biased	$\frac{1}{6}(2u_{i+1} + 5u_i - u_{i-1})$	$\frac{1}{6}(2u_i + 5u_{i+1} - u_{i+2})$

Care was taken above to achieve high order of accuracy for the spatial derivative approximation and not high order approximation to the flux itself. For example, if the exact flux were used at each surface $i+1/2$, $F_{i+1/2} = f_{exact_{i+1/2}}$, then the difference approximation $\frac{F_{i+1/2} - F_{i-1/2}}{\Delta x}$ would be in general only second order accurate. For example, the formula below calculates the left flux to third order accuracy at surface $i+1/2$.

$$F_{L_{i+1/2}} = c\left(u_i + \frac{1}{2}(u_i - u_{i-1}) + \frac{3}{8}(u_{i+1} - 2u_i + u_{i-1}) \right)$$

but the accuracy falls to send order when used to calculate the derivative,

$$\frac{F_{i+1/2} - F_{i-1/2}}{\Delta x} = \frac{\partial u}{\partial x} + \frac{1}{4}\frac{\Delta x^2}{3!}\frac{\partial^3 u}{\partial x^3} + \cdots$$

9.11.2 Example, Higher Order Approximation for Non-Linear Scalar Equations

Instead of the simple wave equation, consider the inviscid Burgers equation, $\frac{\partial u}{\partial t} = -u\frac{\partial u}{\partial x}$. Then we may write it in conservation law form as $\frac{\partial u}{\partial t} = -\frac{\partial f}{\partial x}$, where $f = \frac{u^2}{2}$ with Jacobian $\frac{\partial f}{\partial u} = u$. Splitting the flux according to the sign of the characteristic speed u

$$F_{i+1/2} = \frac{1}{2}\left(1+\text{sgn}(u_L)\right) f_L + \frac{1}{2}\left(1-\text{sgn}(u_R)\right) f_R$$

where the sgn function is given by $\text{sgn}(x) = \begin{cases} 1, & if \quad x \geq 0 \\ -1, & if \quad x < 0 \end{cases}$

Three approximations for first, second and third order accuracy for f_L and f_R for the nonlinear equation are shown in the table below.

Method	f_L	f_R
First order upwind	f_i	f_{i+1}
Second order upwind	$\frac{1}{2}\left(3f_i - f_{i-1}\right)$	$\frac{1}{2}\left(3f_{i+1} - f_{i+2}\right)$
Third order upwind biased	$\frac{1}{6}\left(2f_{i+1} + 5f_i - f_{i-1}\right)$	$\frac{1}{6}\left(2f_i + 5f_{i+1} - f_{i+2}\right)$

The above formulas increased the accuracy of the spatial derivative by using more points to calculate the flux function f. If the variable u was used instead of f in the third order formula at surface $i+1/2$, for example,

$$u_{L_{i+1/2}} = u_i + \frac{1}{2}(u_i - u_{i-1}) + \frac{1}{3}(u_{i+1} - 2u_i + u_{i-1}),$$

then when used to construct $f_{L_{i+1/2}} = \frac{1}{2}u_{L_{i+1/2}}u_{L_{i+1/2}}$ the spatial derivative approximation falls to second order of accuracy.

$$\frac{F_{i+1/2} - F_{i-1/2}}{\Delta x} = \frac{f_{L_{i+1/2}} - f_{L_{i-1/2}}}{\Delta x} = \frac{1}{2}\frac{\partial u^2}{\partial x} + \frac{1}{2}\frac{\Delta x^2}{3!}\frac{\partial u}{\partial x}\frac{\partial^2 u}{\partial x^2} + \cdots$$

9.11.3 Example, Higher Order Approximations for the Euler Equations

Two important considerations for achieving order of accuracy p algorithms were presented within the two subsections above.

1) The approximations to the split flux should be chosen so that when used in the difference equation the spatial derivative is approximated to the desired degree of accuracy. Approximating the flux so that it is of order $p > 2$ at the flux surface $i+1/2$ will in general still limit the accuracy to second order.
2) For nonlinear fluxes, the flux itself should be approximated rather than component factors.

These two considerations will limit the flux calculations for the Euler equations using the flux splitting methods described earlier to second order accuracy at present. Why then are they so popular under this limitation? It is because they can handle shock wave discontinuities well. Modern algorithms often have some form of flux limitation at shock discontinuities that limit the flux to first order accuracy. The overall accuracy of the algorithm will still be of second order because discontinuities occur along only a "thin" set of mesh points.

Consider the Modified Steger-Warming-Version (1), procedure discussed earlier for the nonlinear Euler equations.

$$F_{i+1/2}^{(M-S-W)} = \overline{A}_{+_{i+1/2}} U_L + \overline{A}_{-_{i+1/2}} U_R$$

The practical approach is to approximate U_L and U_R to second or third order of accuracy and then use them to calculate $\overline{A}_{+_{i+1/2}}$ and $\overline{A}_{-_{i+1/2}}$, knowing that the algorithm will be limited to second order accuracy overall. The following table evaluates the variable U to the accuracy indicated at the flux surface $i+1/2$.

Approximation	U_L	U_R
First order upwind	U_i	U_{i+1}
Second order upwind	$\frac{1}{2}(3U_i - U_{i-1})$	$\frac{1}{2}(3U_{i+1} - U_{i+2})$
Third order upwind biased	$\frac{1}{8}(3U_{i+1} + 6U_i - U_{i-1})$	$\frac{1}{8}(3U_i + 6U_{i+1} - U_{i+2})$

For the Roe algorithm $F_{i+1/2}^{(Roe)} = \frac{F_L + F_R}{2} - \frac{1}{2}\left|\hat{A}_{i+1/2}\right|(U_R - U_L)$ or the Modified Steger-Warming-Version (2) procedure, $F_{i+1/2}^{(M-S-W-II)} = \overline{\mathcal{A}}_{+_{i+1/2}} F_L + \overline{\mathcal{A}}_{-_{i+1/2}} F_R$, requiring the evaluation of F_L and F_R, the following table may be helpful.

Method	F_L	F_R
First order upwind	F_i	F_{i+1}
Second order upwind	$\frac{1}{2}(3F_i - F_{i-1})$	$\frac{1}{2}(3F_{i+1} - F_{i+2})$

Third order upwind biased	$\frac{1}{6}\left(2F_{i+1}+5F_i-F_{i-1}\right)$	$\frac{1}{6}\left(2F_i+5F_{i+1}-F_{i+2}\right)$

9.11.4 Stability Considerations

Unfortunately, the simple replacement of the above higher order approximations for spatial derivatives in the previously defined first order Roe or Modified Steger-Warming methods will result in unstable algorithms (see Section 4.4.7). Increasing the order of accuracy of the split flux terms, removes the lowest order dissipation term in the truncation error series, causing an explicit difference method to become unstable. However, when these approximations are used within implicit algorithms, to be discussed later, they can become stable procedures. The next chapter on TVD methods (Total Variation Diminishing) can also use the above higher order flux expressions in stable algorithms. It should also be noted that algorithms using first order in time and higher order spatial approximations are still formally first order methods. However, solutions converging to a steady state can realize the order of accuracy of the higher order spatial approximation.

9.12 Implicit Modified-Steger-Warming and Roe Methods

9.12.1 One Dimensional Implicit Algorithm

In one dimension the implicit Modified-Steger-Warming and Roe methods can be written as

$$\left\{I+\alpha\Delta t\left(\frac{D_-\cdot}{\Delta x}\overline{A}^n_{+_{i+1/2}}+\frac{D_+\cdot}{\Delta x}\overline{A}^n_{-_{i-1/2}}\right)\right\}\delta U_i^{n+1}=-\Delta t\left(\frac{F^n_{i+1/2}-F^n_{i-1/2}}{\Delta x}\right)$$

Note that the split Jacobian matrices, appearing on the left hand implicit side of the equation are the same matrices used to define the explicit Modified-Steger-Warming or Roe flux vector (using $\hat{A}^n_{\pm_{i+1/2}}$ in place of $\overline{A}^n_{\pm_{i+1/2}}$ above for the Roe algorithm). This is in contrast to the implicit unmodified Steger-Warming method, which must use the *true* Jacobians, $\ddot{A}^n_{+_i}=\frac{\partial F^n_{+_i}}{\partial U^n_i}=\frac{\partial A^n_{+_i}U^n_i}{\partial U^n_i}$ and $\ddot{A}^n_{-_{i+1}}=\frac{\partial F^n_{-_{i+1}}}{\partial U^n_{i+1}}=\frac{\partial A^n_{-_{i+1}}U^n_{i+1}}{\partial U^n_{i+1}}$, on the implicit side of the above equation to maintain stability because of the significantly greater dissipation in the method. The modified Steger-Warming and Roe implicit methods need only the much simpler Jacobian matrices on the left hand side for stability balance and are therefore preferred.

We have also introduced a scalar parameter $\alpha\geq 1$ to enhance numerical stability. The implicit equation above represents a block tridiagonal matrix equation, which is given below.

$$\overline{\mathrm{B}}_i\delta U^{n+1}_{i+1}+\overline{\mathrm{A}}_i\delta U^{n+1}_i+\overline{\mathrm{C}}_i\delta U^{n+1}_{i-1}=\Delta U^n_i=-\Delta t\left(\frac{F^n_{i+1/2}-F^n_{i-1/2}}{\Delta x}\right)$$

The block element matrices $\overline{\mathrm{A}}_i$, $\overline{\mathrm{B}}_i$ and $\overline{\mathrm{C}}_i$ are

$$\overline{\mathrm{A}}_i = I + \alpha \frac{\Delta t}{\Delta x}\left(\overline{A}^n_{+i+1/2} - \overline{A}^n_{-i-1/2}\right),$$

$$\overline{\mathrm{B}}_i = +\alpha \frac{\Delta t}{\Delta x}\overline{A}^n_{-i+1/2} \quad \textit{and} \quad \overline{\mathrm{C}}_i = -\alpha \frac{\Delta t}{\Delta x}\overline{A}^n_{+i-1/2}$$

where $\alpha = 1$, for first order flux approximations

and $\alpha \geq \frac{3}{2}$, for higher order flux approximations

The parameter $\alpha > 1$ is chosen to add additional weight to the implicit side to enhance stability.

Figure 9.39 Physics balanced by numerics to achieve stability

Note that the diagonal block matrix element $\overline{\mathrm{A}_i}$ appears to consist of *positive* terms and the two off diagonal block elements look to be *negative*. Thus, the tridiagonal matrix is, in this sense, diagonally dominant.

.

Again the implicit Roe method in one dimension can be given in identical form to that given above for the Modified-Steger-Warming method with *hats* replacing the *bars* on top of the matrix elements. It also has no need of the *true* Jacobians on the implicit side of the equation.

The matrix equation to be solved is

$$\begin{bmatrix} \overline{\mathrm{A}}_I & \overline{\mathrm{C}}_I & 0 & 0 & 0 & 0 & 0 \\ \overline{\mathrm{B}}_{I-1} & \overline{\mathrm{A}}_{I-1} & \overline{\mathrm{C}}_{I-1} & 0 & 0 & 0 & 0 \\ 0 & \ddots & \ddots & \ddots & 0 & 0 & 0 \\ 0 & 0 & \overline{\mathrm{B}}_i & \overline{\mathrm{A}}_i & \overline{\mathrm{C}}_i & 0 & 0 \\ 0 & 0 & 0 & \ddots & \ddots & \ddots & 0 \\ 0 & 0 & 0 & 0 & \overline{\mathrm{B}}_2 & \overline{\mathrm{A}}_2 & \overline{\mathrm{C}}_2 \\ 0 & 0 & 0 & 0 & 0 & \overline{\mathrm{B}}_1 & \overline{\mathrm{A}}_1 \end{bmatrix} \begin{bmatrix} \delta U_I^{n+1} \\ \delta U_{I-1}^{n+1} \\ \vdots \\ \delta U_i^{n+1} \\ \vdots \\ \delta U_2^{n+1} \\ \delta U_1^{n+1} \end{bmatrix} = \begin{bmatrix} \Delta U_I^n \\ \Delta U_{I-1}^n \\ \vdots \\ \Delta U_i^n \\ \vdots \\ \Delta U_2^n \\ \Delta U_1^n \end{bmatrix}$$

Procedures for solving implicit matrix equations are given in the Chapter 11.

9.12.2 Stability Analysis for the Higher Order Implicit Method

Consider the model hyperbolic equation below.

$$\frac{\partial u}{\partial t} + c\frac{\partial u}{\partial x} = 0, \quad with \quad c > 0$$

Applying the implicit method of the last section to this equation with second order accurate spatial difference approximations used on the explicit side, we obtain

$$\left\{1+\alpha c\Delta t\frac{D_{-}^{(1)}\cdot}{\Delta x}\right\}\delta u_i^{n+1}=\Delta u_i^n=-c\Delta t\frac{D_{-}^{(2)}\cdot}{\Delta x}u_i^n=-c\Delta t\frac{3u_i^n-4u_{i-1}^n+u_{i-2}^n}{2\Delta x}$$

$$=-c\Delta t\left\{\underbrace{\frac{u_i^n-u_{i-1}^n}{\Delta x}}_{1^{st}\ order\ \ approx.}+\underbrace{\frac{u_i^n-2u_{i-1}^n+u_{i-2}^n}{2\Delta x}}_{2^{nd}\ order\ \ correction}\right\}$$

where the superscripts on the operators D indicate order of accuracy. Applying the numerical method to an arbitrary Fourier component, we obtain

$$\left\{1+\alpha\frac{c\Delta t}{\Delta x}\left(1-e^{-i\xi}\right)\right\}\delta v_i^{n+1}=-\frac{c\Delta t}{\Delta x}\left(1-e^{-i\xi}\right)\left[1+\frac{1}{2}\left(1-e^{-i\xi}\right)\right]v_i^n$$

where $\xi=k_j\Delta x$, for Fourier wave number k_j. The numerical amplification factor is

$$G_j=1+\frac{-\lambda\left(1-e^{-i\xi}\right)\left[1+\frac{1}{2}\left(1-e^{-i\xi}\right)\right]}{1+\alpha\lambda\left(1-e^{-i\xi}\right)}=\frac{1-\lambda\left[\left(1-e^{-i\xi}\right)+e^{-i\xi}\left(\cos\xi-1\right)\right]+\alpha\lambda\left(1-e^{-i\xi}\right)}{1+\alpha\lambda\left(1-e^{-i\xi}\right)}$$

$$=\frac{1+(\alpha-1)\frac{c\Delta t}{\Delta x}(1-\cos\xi+i\sin\xi)-\frac{c\Delta t}{\Delta x}(\cos\xi-i\sin\xi)(\cos\xi-1)}{1+\alpha\frac{c\Delta t}{\Delta x}(1-\cos\xi+i\sin\xi)}$$

$$=\frac{1+\frac{c\Delta t}{\Delta x}(1-\cos\xi)(\alpha-1+\cos\xi)+\frac{c\Delta t}{\Delta x}i\sin\xi(\alpha-2+\cos\xi)}{1+\alpha\frac{c\Delta t}{\Delta x}(1-\cos\xi)+\alpha\frac{c\Delta t}{\Delta x}i\sin\xi}$$

The magnitude of the amplification factor can be shown to be $\|G_j\|\le 1$ if $\alpha\ge 1$ (Original proof by Stanford Graduate student Yung-Hung Wang). However, a value for α in the range $1<\alpha\le 2$ increases implicit dissipation and is recommended. The magnitudes of the numerical amplification factors for $\alpha=1$ and $\alpha=3/2$ are shown below.

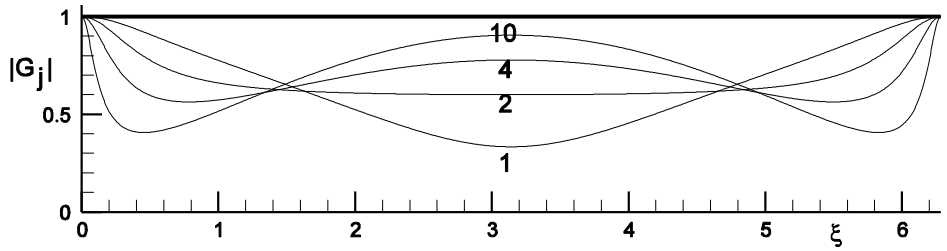

Figure 9.40 $\|G_j\|$ **vs.** ξ**,** $0 \le \xi \le 2\pi$**,** $\alpha = 1$, at CFL numbers 1, 2, 4 and 10

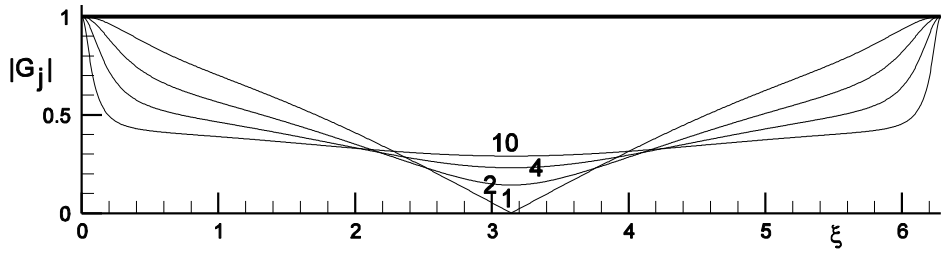

Figure 9.41 $\|G_j\|$ **vs.** ξ**,** $0 \le \xi \le 2\pi$**,** $\alpha = 3/2$, at CFL numbers 1, 2, 4 and 10

Similarly, it can be shown that the third order flux approximation for the explicit spatial derivatives leads to a stable implicit method if $\alpha \ge 1$.

$$\left\{1+\alpha c\Delta t \frac{D_-^{(1)}\cdot}{\Delta x}\right\}\delta u_i^{n+1} = -c\Delta t \frac{D_-^{(3)}\cdot}{\Delta x} u_i^n = -\frac{c\Delta t}{\Delta x}\left\{\frac{2u_{i+1}^n + 5u_i^n + u_{i-1}^n}{6} - \frac{2u_i^n + 5u_{i-1}^n + u_{i-2}^n}{6}\right\}$$

Applying the numerical method to an arbitrary Fourier component, we obtain

$$\left\{1+\alpha\frac{c\Delta t}{\Delta x}\left(1-e^{-i\xi}\right)\right\}\delta v_i^{n+1} = -\frac{c\Delta t}{\Delta x}\left(1-e^{-i\xi}\right)\left[1+\frac{1}{2}\left(1-e^{-i\xi}\right)-\frac{2}{3}\left(1-\cos\xi\right)\right]v_i^n$$

The numerical amplification factor is

$$G_j = 1 + \frac{-\frac{c\Delta t}{\Delta x}\left(1-e^{-i\xi}\right)\left[1+\frac{1}{2}\left(1-e^{-i\xi}\right)-\frac{2}{3}\left(1-\cos\xi\right)\right]}{1+\alpha\frac{c\Delta t}{\Delta x}\left(1-e^{-i\xi}\right)}$$

The magnitudes of the numerical amplification factors for $\alpha = 1$ and $\alpha = 3/2$ are shown below.

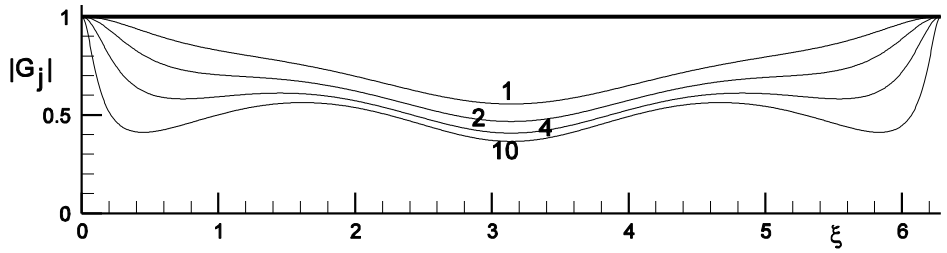

Figure 9.42 $\|G_j\|$ **vs.** ξ**,** $0 \le \xi \le 2\pi$**,** $\alpha = 1$, at CFL numbers 1, 2, 4 and 10

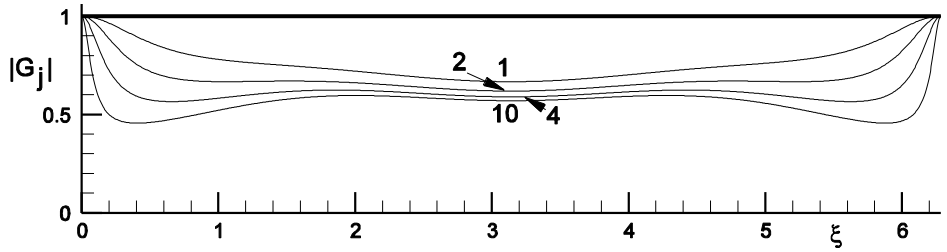

Figure 9.43 $\|G_j\|$ **vs.** ξ**,** $0 \le \xi \le 2\pi$**,** $\alpha = 3/2$, at CFL numbers 1, 2, 4 and 10

9.12.3 Two Dimensional Implicit Algorithm

$$\underbrace{\left\{ I + \alpha\Delta t\left(\frac{D_-}{\Delta x}\cdot\overline{A}^{n}_{+_{i+1/2,j}} + \frac{D_+}{\Delta x}\overline{A}^{n}_{-_{i-1/2,j}} + \frac{D_-}{\Delta y}\cdot\overline{B}^{n}_{+_{i,j+1/2}} + \frac{D_+}{\Delta y}\cdot\overline{B}^{n}_{-_{i,j-1/2}} \right) \right\} \delta U^{n+1}_{i,j}}_{NUMERICS} = \Delta U^{n+1}_{,i,j}$$

$$= \underbrace{-\Delta t\left(\frac{F^n_{i+1/2,j} - F^n_{i-1/2,j}}{\Delta x} + \frac{G^n_{i,j+1/2} - G^n_{i,j-1/2}}{\Delta y} \right)}_{PHYSICS}$$

where $\alpha = 1$, for first order flux approximations
and $\alpha \ge \dfrac{3}{2}$, for higher order flux approximations.

Similarly, the block element matrices are now defined as follows.

$$\overline{\mathrm{A}}_{i,j} = I + \alpha\frac{\Delta t}{\Delta x}\left(\overline{A}^{n}_{+_{i+1/2,j}} - \overline{A}^{n}_{-_{i-1/2,j}}\right) + \alpha\frac{\Delta t}{\Delta y}\left(\overline{B}^{n}_{+_{i,j+1/2}} - \overline{B}^{n}_{-_{i,j-1/2}}\right),$$

$$\overline{\mathrm{B}}_{i,j} = +\alpha\frac{\Delta t}{\Delta y}\overline{B}^{n}_{-_{i,j+1/2}}, \qquad \overline{\mathrm{C}}_{i,j} = -\alpha\frac{\Delta t}{\Delta y}\overline{B}^{n}_{+_{i,j-1/2}},$$

$$\overline{\mathrm{D}}_{i,j} = +\alpha\frac{\Delta t}{\Delta x}\overline{A}^{n}_{-_{i+1/2,j}} \quad \textit{and} \quad \overline{\mathrm{E}}_{i,j} = -\alpha\frac{\Delta t}{\Delta x}\overline{A}^{n}_{+_{i-1/2,j}}$$

It is important to note that, although the spatial approximation of the derivatives appearing on the right hand side of the equation can be higher than first order, only first order accurate special approximations are used on the left hand, or implicit side. To raise the order of accuracy of the implicit side would be costly in that more diagonals would be added to the implicit matrix equation to be solved and simple efficient block tridiagonal inversion could no longer be used. The implicit side is first order accurate in both space and time. However, if the solution goes to a steady state, the principal reason for using large implicit time steps, the solution will have the high order of accuracy of the explicit, or left hand, side of the equation.

9.13 Higher Order Time Accuracy

Consider the following equation in conservation law form

$$\frac{\partial U}{\partial t} = -\frac{\partial F}{\partial x} - \frac{\partial G}{\partial y} = R(U)$$

where $R(U)$ represents the right hand side of the equation. For an equation going toward a steady state, $R(U)$ would represent the residual which is to be driven to zero. An implicit algorithm, for example that shown in Section 9.11.3, may be written as follows

$$\underbrace{\left\{ I + \Delta t \left(\frac{D \cdot \overline{\ }}{\Delta x} \overline{A} + \frac{D_{-} \cdot \overline{\ }}{\Delta y} \overline{B} \right) \right\} \delta U_{i,j}^{n+1}}_{NUMERICS} = \underbrace{-\Delta t \left(\frac{F_{i+1/2,j}^{n} - F_{i-1/2,j}^{n}}{\Delta x} + \frac{G_{i,j+1/2}^{n} - G_{i,j-1/2}^{n}}{\Delta y} \right)}_{PHYSICS} = \Delta t \; R_{i,j}^{n}$$

We may also express this more concisely as

$$\left\{ I - \Delta t \left. \frac{\partial R}{\partial U} \right|_{i,j}^{n} \right\} \delta U_{i,j}^{n+1} = \Delta t \; R_{i,j}^{n}$$

If the time step Δt is chosen very large, then the above equation becomes Newton's method for finding $U_{i,j}^{n+1}$ such that $F(U_{i,j}^{n+1}) = 0$.

$$U_{i,j}^{n+1} = U_{i,j}^{n} - \left(\left. \frac{\partial R}{\partial U} \right|_{i,j}^{n} \right)^{-1} R_{i,j}^{n}, \quad n = 1, 2, 3, \cdots$$

This is the fastest way to obtain steady state solutions. However, for unsteady solutions an accurate time history of the solution is sought. The time derivative can be approximated by

$$\left. \frac{\partial U}{\partial t} \right|_{i,j}^{n+1} \simeq (1+\varphi) \frac{U_{i,j}^{n+1} - U_{i,j}^{n}}{\Delta t} - \varphi \frac{U_{i,j}^{n} - U_{i,j}^{n-1}}{\Delta t}$$

If $\varphi = 0$ this approximation is first order accurate in time and if $\varphi = 1/2$ it is second order accurate. The equation to be solved is then

$$(1+\varphi)\frac{U_{i,j}^{n+1} - U_{i,j}^{n}}{\Delta t} - \varphi\frac{U_{i,j}^{n} - U_{i,j}^{n-1}}{\Delta t} = R(U_{i,j}^{n+1}) = R(U_{i,j}^{n+1}) + \left.\frac{\partial R}{\partial U}\right|_{i,j}^{n} \delta U_{i,j}^{n+1}$$

This equation can be solved efficiently by sub-iteration using the same implicit procedures as before. Note the sub-iteration indices (k) and (k+1) in the equations below

$$(1+\varphi)\frac{U_{i,j}^{(k+1)} - U_{i,j}^{n}}{\Delta t} - \varphi\frac{U_{i,j}^{n} - U_{i,j}^{n-1}}{\Delta t} = R(U_{i,j}^{(k+1)})$$

where $U_{i,j}^{(1)} = U_{i,j}^{n}$ and as $k \to \infty$, $U_{i,j}^{(k+1)} \to U_{i,j}^{n+1}$. The above equation can be expressed as

$$(1+\varphi)\frac{U_{i,j}^{(k+1)} - U_{i,j}^{(k)} + U_{i,j}^{(k)} - U_{i,j}^{n}}{\Delta t} - \varphi\frac{U_{i,j}^{n} - U_{i,j}^{n-1}}{\Delta t} = R(U_{i,j}^{(k)}) + \left.\frac{\partial R}{\partial U}\right|_{i,j}^{(k)} (U_{i,j}^{(k+1)} - U_{i,j}^{(k)})$$

or

$$(1+\varphi)\frac{U_{i,j}^{(k+1)} - U_{i,j}^{(k)}}{\Delta t} = R(U_{i,j}^{(k)}) + \left.\frac{\partial R}{\partial U}\right|_{i,j}^{(k)} (U_{i,j}^{(k+1)} - U_{i,j}^{(k)}) + \varphi\frac{U_{i,j}^{n} - U_{i,j}^{n-1}}{\Delta t} - (1+\varphi)\frac{U_{i,j}^{(k)} - U_{i,j}^{n}}{\Delta t}$$

or, finally as

$$\underbrace{\left\{ I + \frac{\Delta t}{1+\varphi}\left.\frac{\partial R}{\partial U}\right|_{i,j}^{(k)} \right\}}_{NUMERICS} \delta U_{i,j}^{(k+1)} = \frac{\Delta t}{1+\varphi} \underbrace{\left\{ R(U_{i,j}^{(k)}) - (1+\varphi)\frac{U_{i,j}^{(k)} - U_{i,j}^{n}}{\Delta t} + \varphi\frac{U_{i,j}^{n} - U_{i,j}^{n-1}}{\Delta t} \right\}}_{NEW\ RIGHT\ HAND\ SIDE\ RESIDUAL\ \ R'}$$

where $\delta U_{i,j}^{(k+1)} = U_{i,j}^{(k+1)} - U_{i,j}^{(k)}$. The right hand side residual R' now approximates the complete unsteady equation, $-R'(U) \approx \frac{\partial U}{\partial t} + \frac{\partial F}{\partial x} + \frac{\partial G}{\partial y}$, to perhaps a high order of accuracy in both time and space.

This equation can be rewritten to appear like a standard implicit equation, using $\Delta\tau = \frac{\Delta t}{1+\varphi}$,

$$\left\{ I + \Delta\tau\left.\frac{\partial R}{\partial U}\right|_{i,j}^{(k)} \right\} \delta U_{i,j}^{(k+1)} = \Delta\tau R'(U_{i,j}^{(k)})$$

The above equation is solved in pseudo time τ with as large a pseudo time step $\Delta\tau$ as possible and in as few sub-iteration steps as necessary to converge $U_{i,j}^{(k+1)} \to U_{i,j}^{n+1}$ and the residual R' to near zero. The convergence criterion should be about $\left|\delta U_{i,j}^{(k+1)} / U_{i,j}^{(k+1)}\right| \approx 0.05$. Thus, the same

implicit procedure used to converge to steady state solutions is used now to converge to the unsteady solution $U_{i,j}^{n+1}$ in pseudo time during each time step Δt. The maximum value for k should be about 5. If too much action takes place during a single time step, needing many sub-iterations for convergence, Δt should be reduced. Algorithms for solving implicit matrix equations are discussed in Chapter11.

9.14 Some Concluding Remarks

The algorithms presented within this chapter displayed numerical difficulties. The first order algorithms were for the most part non-oscillatory, but they washed out discontinuities in the flow, more so for the linear or nearly linear discontinuities, such as contact discontinuities or discontinuities in slope, such as the leading and trailing edges of rarefactions. There were some bright occurrences, such as the ability of the Roe method to treat stationary shock waves. All the second order accurate algorithms, as is their nature, showed oscillations, some requiring artificial viscosity to damp out unwanted numerical disturbances. The next chapter on high resolution algorithms will remove these disturbances while maintaining high order of accuracy.